Title
HYPERFINE-STRUCTURE MEASUREMENTS ON RUBIDIUM-81 AND 82

Author
Faust, John Daly.

Publication Date
1961-09-30

UCRL-9874
UC-34 Physics
TID-4500 (16th Ed.)

UNIVERSITY OF CALIFORNIA

Lawrence Radiation Laboratory
Berkeley, California

Contract No. W-7405-eng-48

HYPERFINE-STRUCTURE MEASUREMENTS ON RUBIDIUM-81 AND -82

John Daly Faust

(M. A. Thesis)

September 30, 1961

Printed in USA. Price $1.25. Available from the
Office of Technical Services
U. S. Department of Commerce
Washington 25, D.C.

HYPERFINE-STRUCTURE MEASUREMENTS ON RUBIDIUM-81 AND -82

Contents

DISCLAIMER

HYPERFINE-STRUCTURE MEASUREMENTS ON RUBIDIUM-81 AND -82

John Daly Faust

Lawrence Radiation Laboratory
University of California,
Berkeley, California

September 30, 1961

ABSTRACT

The atomic-beam magnetic-resonance method has been used to measure the hyperfine-structure separation in two neutron-deficient isotopes of rubidium, Rb^{81} and Rb^{82}. In the $^2S_{1/2}$ electronic state, observation of $\Delta F = \pm 1$ lines at very low field values allows very accurate determination of $\Delta \nu$. The following values were obtained:

$$\Delta \nu_{81} = 5111.589 \pm .040 \text{ Mc}$$

$$\Delta \nu_{82} = 3094.084 \pm .006 \text{ Mc}.$$

Details of construction of the apparatus are presented along with a brief outline of the theory of the hyperfine interaction.

the atomic-beams magnetic-resonance method. The biggest virtue of the atomic-beams method derives from the fact that each atom traverses the length of the resonant apparatus in complete isolation from its neighbors. The perturbing influence of crystalline fields and neighbor-neighbor interactions is absent. So data gathered by atomic-beams methods should be free of corrections from these effects.

The theory will be described in greater detail in Section III, but in brief, single atoms as they travel through various magnetic and radiofrequency electromagnetic fields are separated spatially into their electronic and nuclear magnetic substates. The displacement due to the electronic moment is very much larger than that due to the nuclear moment, and in fact, is large enough to cause a physical separation of the beam into two parts. Each of these parts travels a separate path through the magnetic fields. The initial directions of the two paths are so directed by the fields and by a set of defining slits that both paths occupy the same space when they arrive within the resonant region. If the combination of the magnetic field in the resonant region and the frequency of the electromagnetic field there are correct, a transition from one substate to another can occur; if the transition is from one electronic state to the other, regardless of the magnetic nuclear substate transition, the subsequent path of the atom is altered enough for the transition to be detected. Observation of the beam at the detector as the radiofrequency field is changed enables us to determine the rf spectrum of the atom. From this we can determine the hyperfine interaction constants.

Section II deals with the design of the apparatus, incorporating recent changes in design. Sections III, IV, and V deal with the experiment itself: Section III develops the theory of the hyperfine interaction, Section IV describes the experimental techniques, and Section V outlines the experimental results.

II. APPARATUS DESIGN

The apparatus consists of an oven for producing the beam, a series of magnets for deflecting it, a series of collimating slits, and a detector. All these are contained within a large steel tank with various pumps attached to produce a vacuum. Figure 1 is an over-all view of the apparatus; Fig. 2 shows placement of the various parts. The machine in its present stage is described in detail in the thesis of N. Braslau (BRA 60). Only minor changes to improve the vacuum system have been incorporated since that time. However, a short description of each major component will be included for completeness.

A. Over-all Design and Dimensions

The machine is designed symmetrically about the center of the C-magnet because the A- and B-magnets are of equal length. The beam height at the detector is 1 cm. With the length of the A- and B-magnets as 44.45 cm, and the design equations from the thesis of R. J. Sunderland (SUN 56), the total length of the apparatus from oven slit to button loader is 194.03 cm, with the exit-slit detector 7 cm in front of the button loader. The outside length of the tank is about 85 in. (203 cm).

B. Ovens and Oven Loaders

One of the disadvantages to the type of oven-loader system used by Braslau (Fig. 5, BRA 60) was that the water lines were connected from the stationary plate to the moveable oven loader inside the vacuum. In order to adjust the position of the oven for maximum transmission, the water lines had to be made flexible. This was done at first merely by making the copper lines quite long and wrapping them around the body of the column, thus relying on the flexibility of the copper. As time went on, it became necessary to replace the rubber O-rings which maintained the vacuum between the tank proper and atmospheric pressure. In doing so, the lines had to be stretched beyond their elastic limit, and in

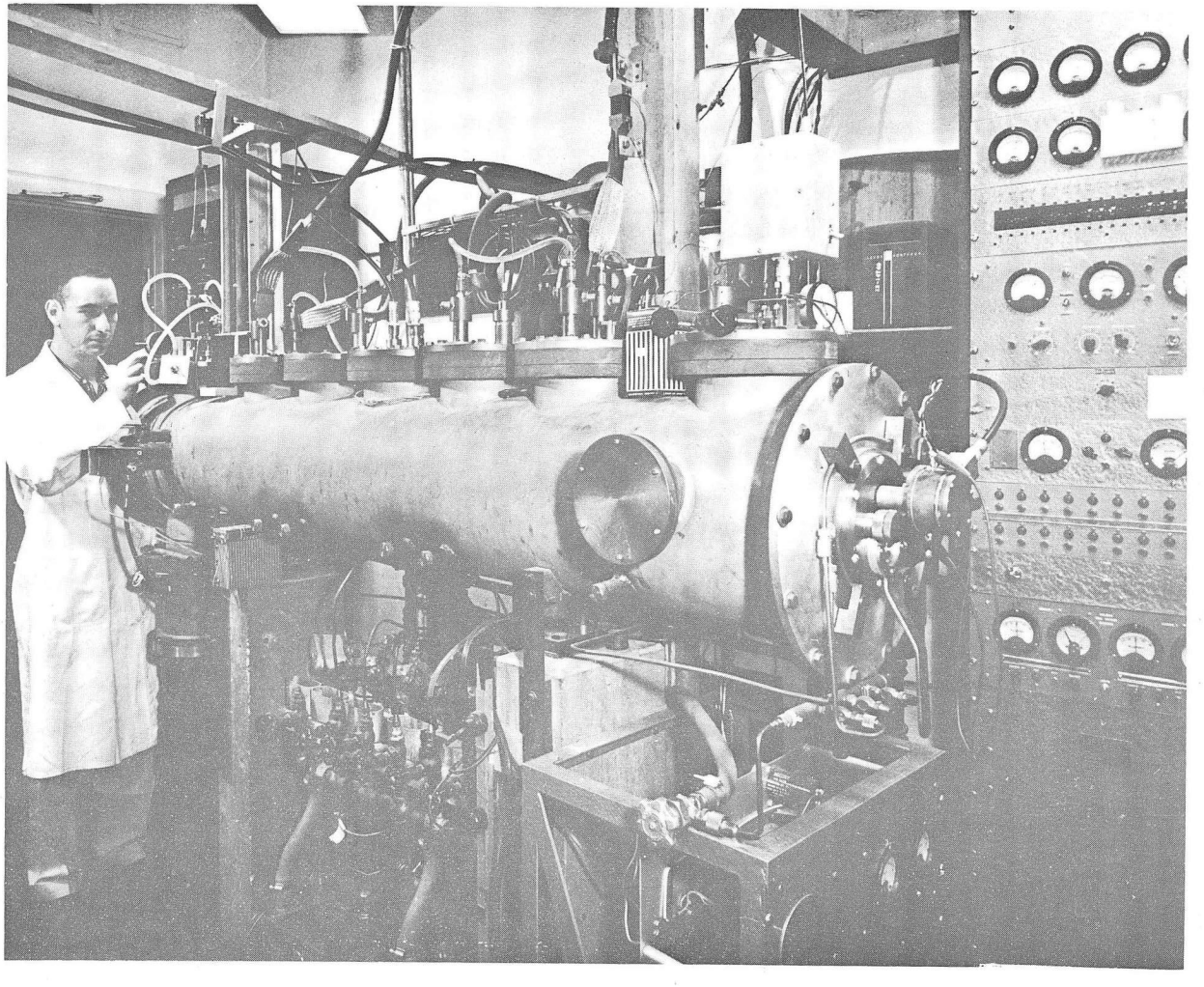

ZN-2055

Fig. 1. An over-all view of the apparatus from the button-loader (detector) end.

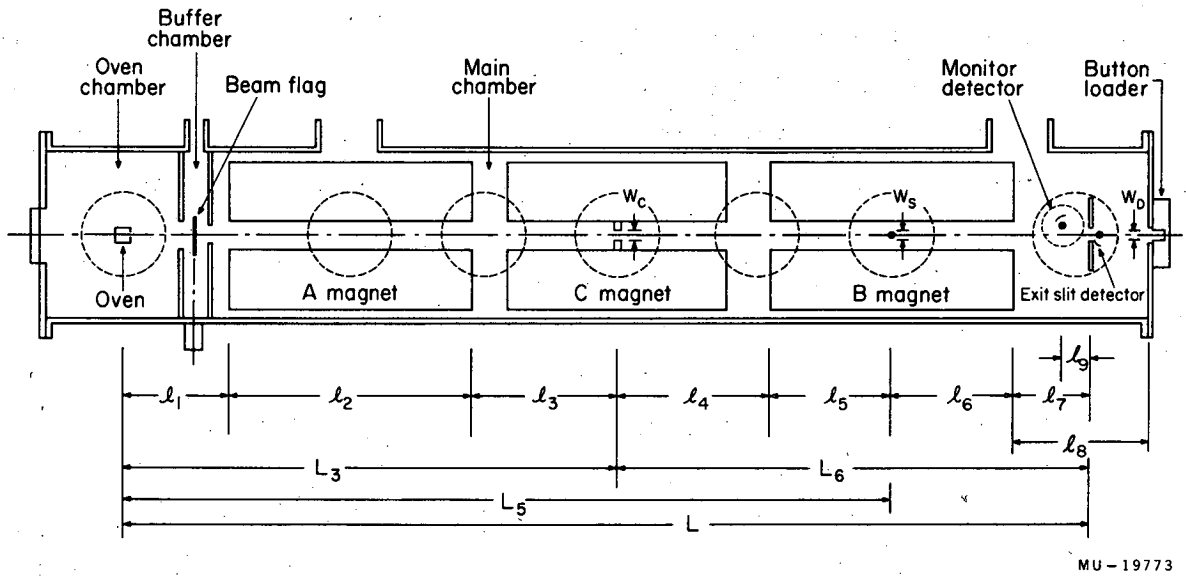

Fig. 2. A schematic of the atomic-beam apparatus.

attempting to realign them, some leaks developed which required replacing the flexible system. Sylphons were tried, but the vacuum problems were too great. Eventually a new design of oven loader which would be compatible with the old plunger was developed. External hoses provided the required flexibility (Fig. 3).

The final design of the oven was a combination of previous designs, combining a long thin circular hole from the cavity of the block to the slits, and slits which were 1/8 inch thick separated by 5 mils. This arrangement gave slightly better collimation than that from an infinitely high slit 125 mils deep by 5 mils wide. Figure 4 is a photograph of a disassembled oven. Several designs with greater collimation were tried, but no further improvement in efficiency was noted. (A typical collimated oven consisted of three vertical slits, one above the other, separated by a partition about 1 to 3 mils thick. Each slit was 125 mils deep, 20 mils high, and from 1 to 15 mils wide.) More experimentation in collimation is in progress.

The ovens were heated by electron bombardment from a U-shaped thoriated-tungsten filament which had been coated with Aquadag, an aqueous suspension of carbon. The carbon lowers the work function of the wire by forming ThC and WC which have low work functions. This allows electron emission at a lower temperature, increasing filament life. A small piece of nickel is spot welded to each end of the filament and is in turn spot welded to each of two steel blocks. It is difficult to get the tungsten wire to stick to the steel directly, and it is expensive to have the blocks milled entirely from nickel. The filament is extremely brittle once it has been heated, and consequently is easily and often broken.

The filament is heated to about 1500°C by a power supply providing about 11 amp. At this temperature electron emission occurs, and the electrons can be accelerated into the oven, which is held at positive potential up to 300V. The oven heating can be controlled by varying the potential difference between the filament and the oven. Three-hundred volts seems to be a practical maximum before arcing occurs at the usual pressures in the oven chamber.

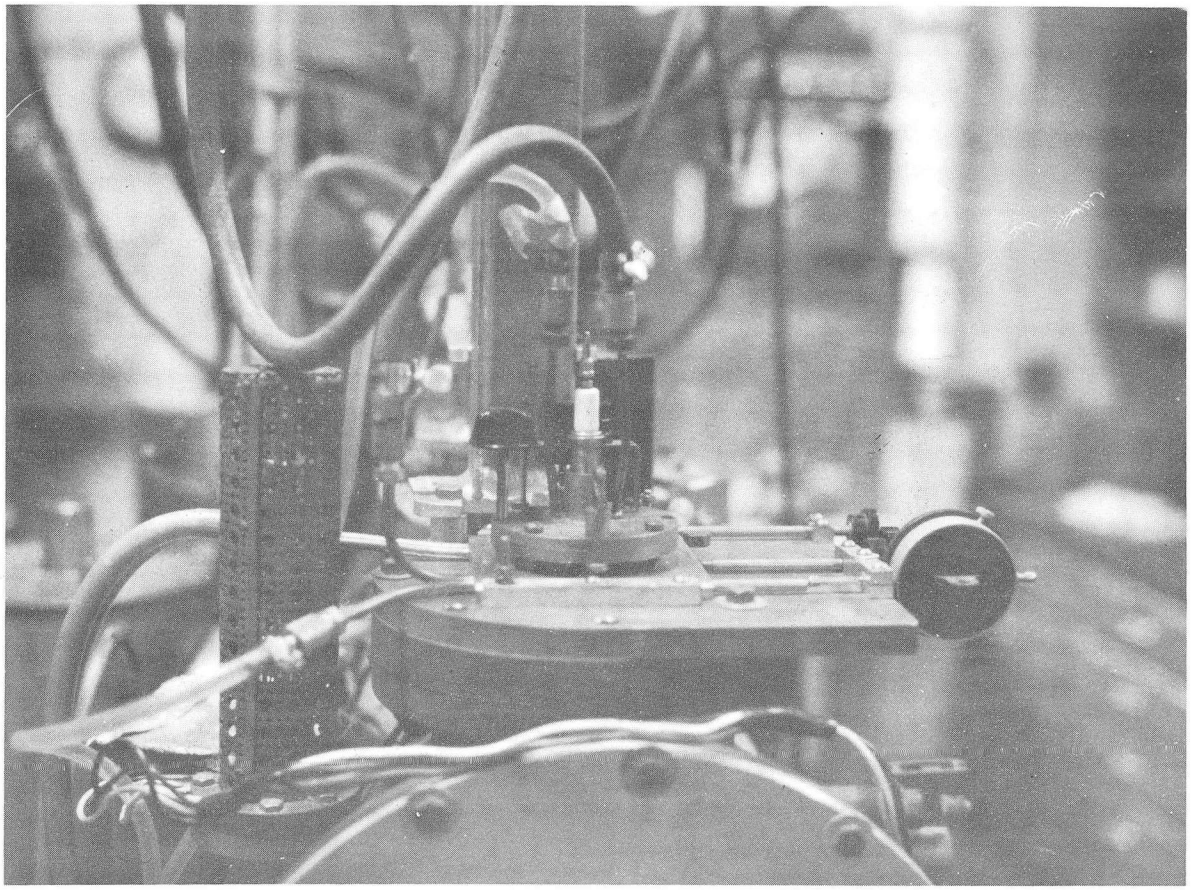

ZN-2961

Fig. 3. The new oven loader without flexible couplings in the vacuum.

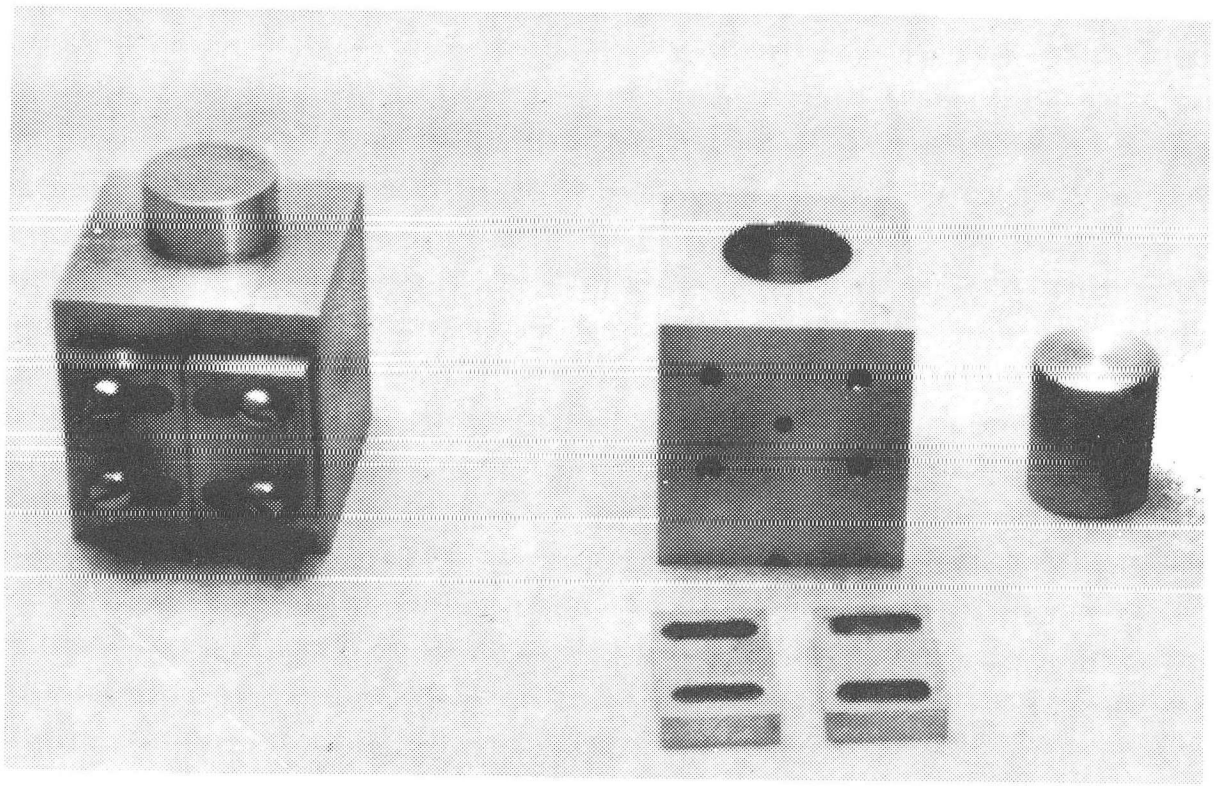

ZN-2962

Fig. 4. The oven assembly.

C. The Magnet System

The magnet system consists of two inhomogeneous magnets, the A- and B-magnets--used for deflecting the beam and separating it into two groups of energy states--and an adjustable homogenous magnet for maintaining the orientation of the states and placing them into an exactly determined field in order to permit radiofrequency (rf) transitions from one group of states to the other. All three magnets are described in great detail with pictures in Braslau's thesis (BRA 60) and elsewhere (SUN 56, BEM 53). The A- and B-magnets have cylindrical-type pole faces (Fig. 5); both are identical except for a vertical slot in the B-magnet for the stopwire. The C-magnet has a pair of parallel surfaces separated by 1/4 in., between which the rf hairpins can be placed. The directions of the A- and B-fields are arranged in the "flop-in" manner first described by Zacharias (ZAC 42) so that no signal is detected unless a transition occurs from one of the energy groups to the other (see Section II C). The flop-in method is absolutely imperative in radioactive work with short-lived isotopes because in this case a signal represents a large percentage change in counting rate. The stopwire design was improved slightly by adding another O-ring to the plunger.

Power for the A- and B-magnets is supplied by twelve 2v submarine storage batteries connected in series parallel to give 4v at 350 amp. The current is turned on or off with a knife switch. The inhomogeneities of the fields produced are about 5000 gauss/cm.

The C-magnet current is supplied by two of the same kind of submarine batteries connected in series with a bank of resistors and a 5-amp feedback system. The feedback is controlled by a rather complicated electronic servomechanism capable of keeping the magnetic field locked on a resonace of any stable isotope having an observable transition at that field. A detailed description is beyond the scope of this paper (See BRI 59).

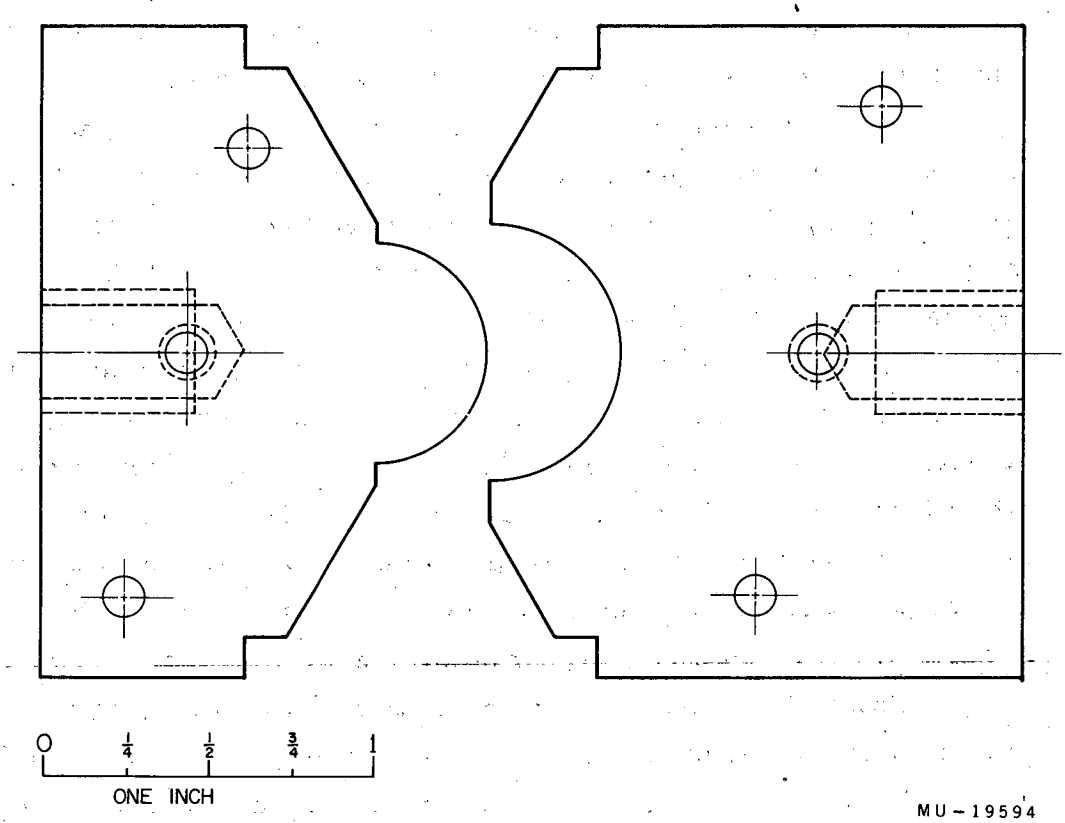

Fig. 5. The pole faces of the A and B magnets.

D. The Collimating Slits, Stopwire and Beam Flag

Immediately after the atoms leave the oven slits, they pass through two pairs of slits that buffer the high pressure of the oven chamber from the lower pressure of the main chamber containing the magnets and the detection systems. These slits are about 1/4 in. wide and 1/2 in. high, which allows the beam to pass but permits a differential pressure to be maintained. In the buffer chamber, which is only about 2 in. long, is a beam flag--a metal plate that can be inserted into the beam to shut it off. The cylindrical plunger that actuates the flag slides on three O-ring seals to insure good vacuum isolation.

In the center of the C-magnet is the collimator slit (Fig. 6), which provides the central point of symmetry of the machine. It is placed at the position in the C-magnet where the two paths of atoms cross. On both sides of this collimator are placed the various rf hairpins, with the Ramsey hairpin straddling the collimator.

In the center of the B-magnet is the movable stopwire (Fig. 7) which serves to cut down the number of fast atoms and molecules that go through the apparatus without being deflected sufficiently to be thrown out of the undeflected beam path(the beam path is the path the atoms would traverse if the magnets were off and the only obstruction was the collimator). The 56-mil width of the stopwire is just that of the undeflected beam after it has passed through the collimator.

The final slit that defines the beam is the exit slit. This can be moved back and forth until an optical light ray from a point source at the oven position just going inside the collimator and just outside the stopwire will be stopped on both sides. Actually, the light coming from the oven filament is extended over the width of the buffer slits; the exit slit is adjusted to make an equal amount of light pass on either side of the stopwire. A window has been provided in one of the positions of the button loader for this adjustment.

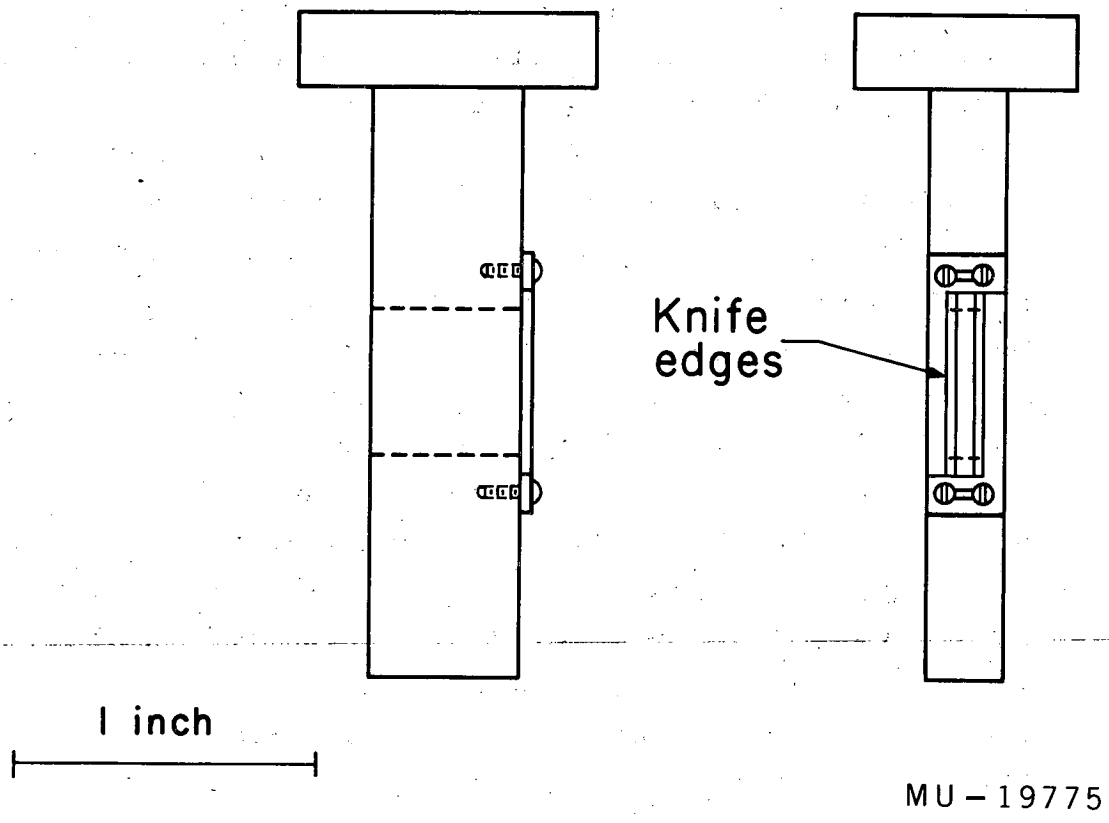

Fig. 6. The collimator slit.

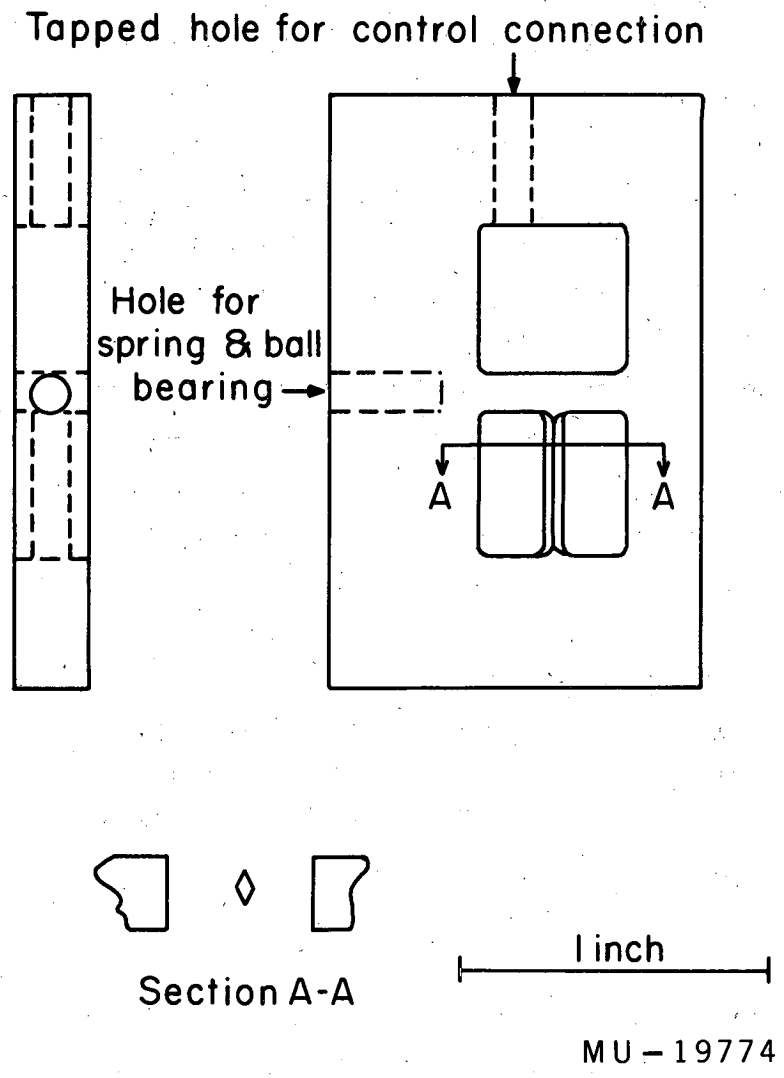

Fig. 7. The movable stopwire plate.

E. The Detectors

There are two types of detectors for the two kinds of atoms we must detect--hot-wire detectors for the intense (10^{-9}-amp) beams of stable material used for locking and calibration, and sulfur-coated buttons for the very weak (10^{-16} amp) beams of radioactive isotopes. The numbers of radioactive atoms are such a small percent of the total beam that the hot wire is completely insensitive to the radioactive species, and the method of detection of the radioactive beam makes it completely insensitve to the numbers of stable atoms simultaneously collected.

The hot-wire detectors are 10-mil potassium-free tungsten wires mounted vertically in two places in the beam. Closest to the oven, and just behind the B-magnet is the monitor detector; just beyond that is the exit or locking detector. Mounted near each hot wire is the collector, a small copper plate 1 cm by 1 cm, which is held at ground potential. The wire is heated until it glows dull red by an automobile storage battery supplying about 1 amp through a controlling resistance. Alkali atoms which impinge on the hot wire come off as positve ions because the work function of tungsten is greater than the ionization potential of the alkali metals. The positive ions thus formed are than attracted to the grounded plate. The hot wire is kept at a positive potential of 4 to 45 v. An electrometer such as the vibrating-reed, capacitor type, Beckman Model-5 micromicroammeter is used to measure the positive-ion current.

The monitor detector is placed so that, when the A- and B-magnets are turned on and the stopwire inserted, the filament of the detector is at the place of maximum intensity of the "thrown-out" beam. It has been found that the intensity of the thrown-out beam is directly proportional to the full beam intensity.

The monitor detector can also be moved to the center of the machine to be used as a calibration resonance indicator. At this position in the beam path the two paths of refocused atoms have not completely come together, and the best position of the filament is found

to be slightly to one side or the other of the machine center line. This method of calibration was found superior to a method previously used involving a third and much wider hot wire mounted on the button loader. Flopped-out beam levels of 3×10^{-11} amp as measured by the monitor detector, were found to give marginally satisfactory intensities for operating the locking detector. Levels of 10×10^{-11} were completely satisfactory.

The locking detector is attached to the exit slit in such a way as to be still in the "flopped-in" beam, but not to be at the place of maximum intensity. Since the locking detector is attached directly to the exit slit, the detector is not used to position the slit, rather, the slit is lined up optically as previously described. Figure 8 shows the cylindrical shield surrounding the monitor detector, and Fig. 9 shows the exit slit and its detector as seen looking toward the oven.

Sulfur-coated buttons placed directly into the vacuum at the beam focus are used to collect the radioactivity. The rubidium atoms--stable and radioactive alike--stick to the sulfur. After exposure, the buttons are removed from the vacuum and placed in a NaI scintillation counter. The K X-rays from the resulting daughter krypton-81 and -82 strike the thin NaI crystal, causing a burst of light which is amplified by a photomultiplier tube. The bursts are counted by a binary counter. Needless to say, the stable atoms have no effect on the counters. Full beam intensities up to 1000 cpm are possible with corresponding resonance buttons of 10 to 20 cpm, although in this work one third of the above counting rates were more usual.

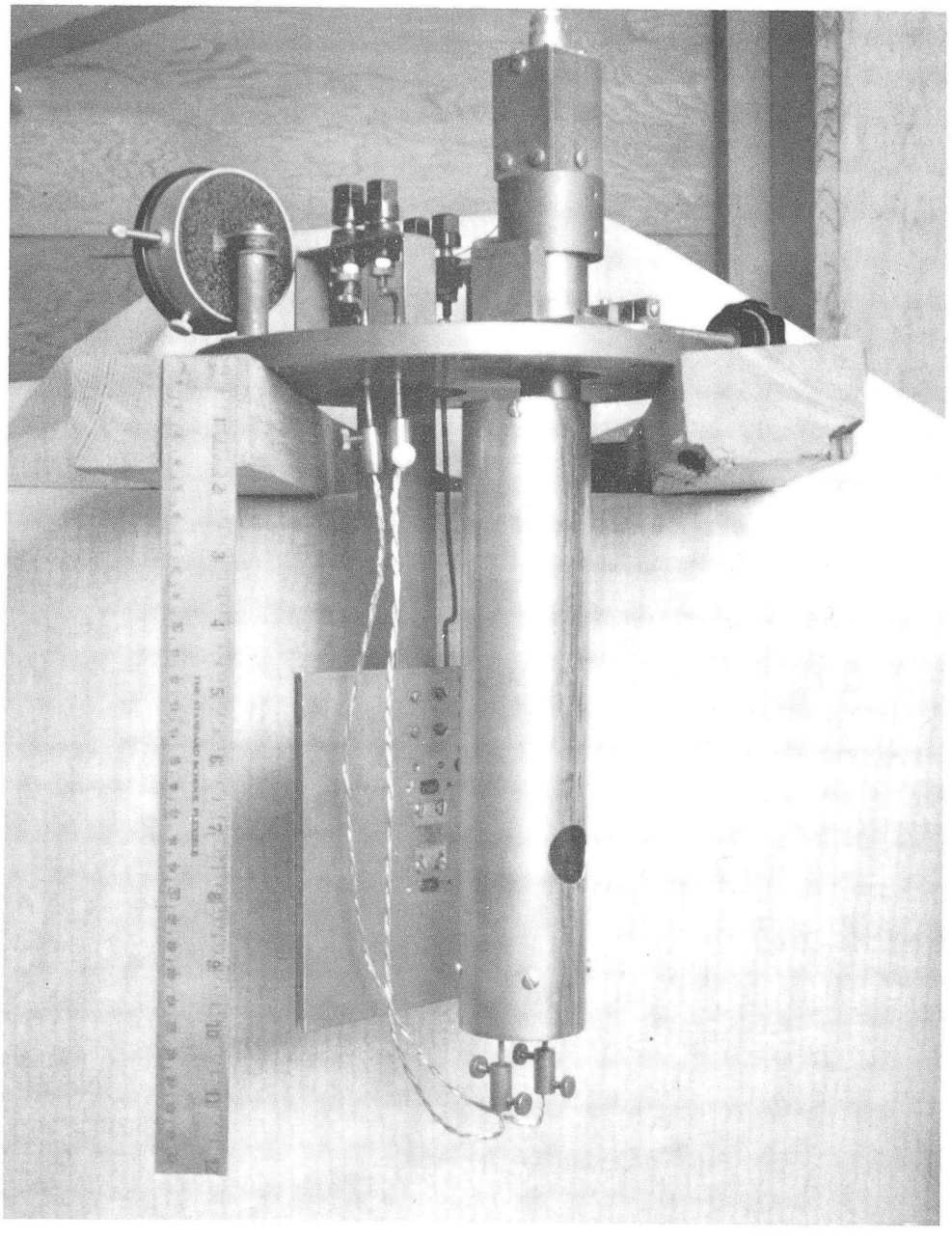

ZN-2388

Fig. 8. The monitor detector.

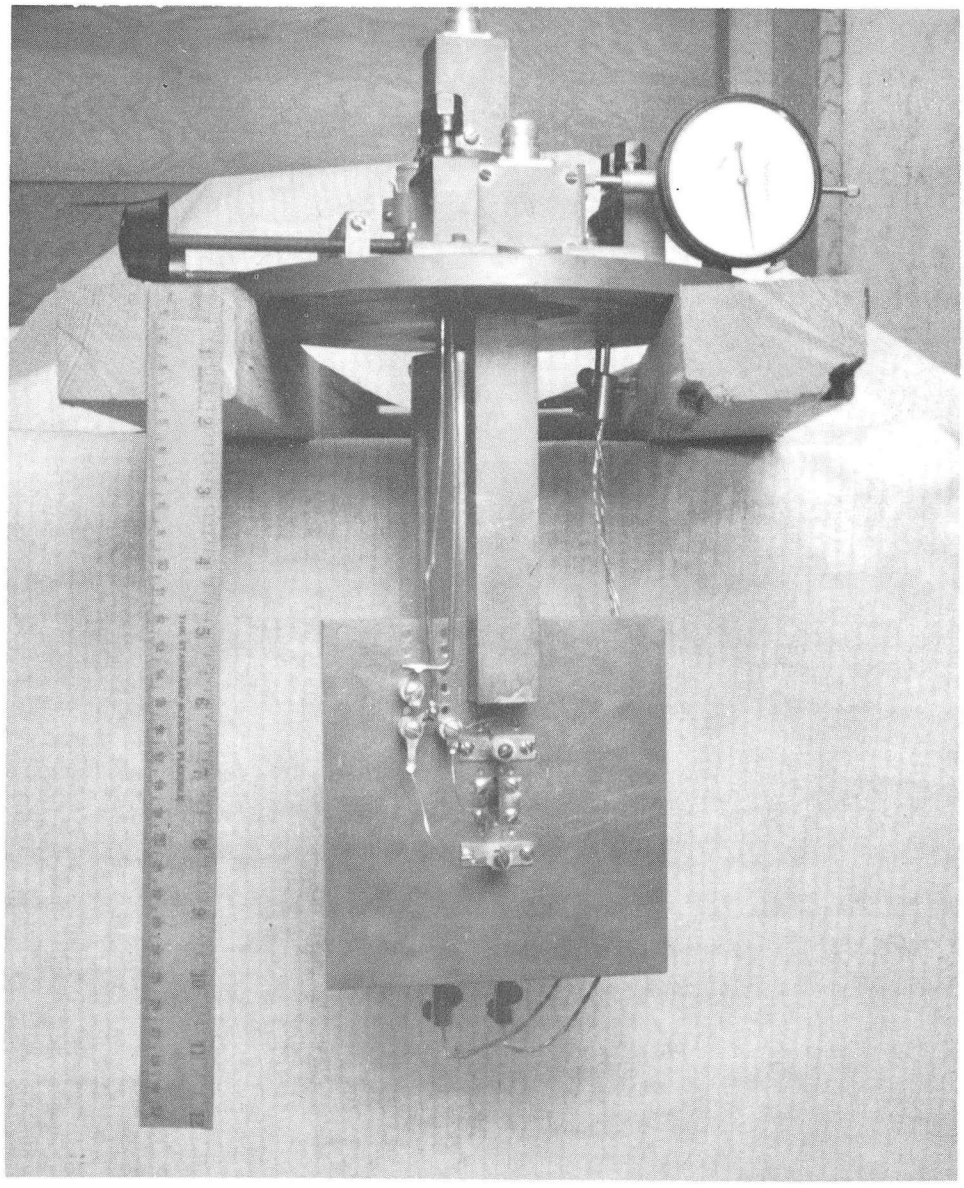

ZN-2387

Fig. 9. The exit slit and its detector.

F. The Vacuum System

The vacuum system consists of several high-speed oil-diffusion pumps pyramided above a single mechanical pump, itself capable of maintaining a vacuum of less than 300 microns. The mechanical pump is fed from two 300-cfm oil pumps, one of which backs two 700-cfm pumps which evacuate the main chamber, the other which backs another 700-cfm pumping the oven chamber and a smaller 260 cfm pumping the buffer chamber. The three 700-cfm pumps and the 260-cfm pump have liquid-nitrogen traps mounted between them and the tank. The cold surface provided by the nitrogen cooled jacket condenses oil vapor from the trap before it reaches the interior of the can. The sides of the pumps are cooled with running water; an interlocking system prevents the pumps from running in case of water-pressure failure. A similar system stops the diffusion pumps to prevent oxidation of the oil whenever the pressure becomes greater than 200 microns. However, since the pumps do keep running for some minutes after they are turned off, it was found helpful to use a special silicone vacuum-pump oil, Dow Corning 704, which does not oxidize as readily as petroleum-based oils.

With the oven off, pressures of 2 to 3×10^{-7} mm Hg were attained. With the oven pouring out a beam of alkali atoms, the pressures were usually about 10^{-6} mm in the main chamber and five times that in the oven chamber. The mean free path at 5×10^{-6} mm is 60m, and so the beam suffers little attenuation from gas scattering.

G. The Radiofrequency System

According to the quantum theory, the amount of energy received by an atom must exactly equal (within the uncertainty principle) the energy required to cause the transition. The method of applying the energy in atomic beams is by means of radiofrequency quanta. The beam of atoms passes through a region, the hairpin, which has a high density of quanta of the proper energy. The intensity is not critical within a fairly wide range, although too great an intensity will cause

some of the atoms that have accepted a quanta to re-emit, with a resulting decrease in the number of atoms that have changed from one state to another. Electromagnetic radiation of the required energy is generated by a primary source that can produce frequencies from 20 to 40 Mc/sec and a multiplier that holds a stable frequency from 500 to 1000 Mc/sec locked to the signal from the primary source. This intermediate frequency (500 to 1000 Mc/sec) is then multiplied into the proper range, usually about 3 to 5 kMc/sec, and amplified to achieve the necessary intensities.

Three frequencies are needed-one for locking the C-field, one for calibrating that field, and a third for the actual search for the transition energy. The second and third are not used simultaneously, since the same hairpin is used in the calibration as in the search. Thus, except for times when a simpler method to calibrate can be used, we need at most two simultaneous frequency sources.

The frequency sources used in this experiment are almost identical to each other, the only slight difference being in the locking system for a reason peculiar to the locking method. (See BRI 59 for a detailed description of the method of locking.) The basic frequency sources are AM-1 interpolators made by Gertsch Products, Inc., Los Angeles, California.

The AM-1 interpolator is a phase-locked oscillator in which a very accurate 100-kc signal is multiplied to 1 and 10 Mc; the 1-Mc signal is multiplied to 19 to 38 Mc in a variable multiplier. This signal is then mixed with that from a free-running 1-to 2-Mc oscillator, whose frequency is read by a Hewlett-Packard frequency counter. The upper side band of the mixer output is fed to a buffer amplifier, which locks a 20- to 40-Mc oscillator to this frequency. The amplified signal is sent through a crystal diode from which harmonics up to the kilomegacycle range are obtained. This harmonic-rich signal is fed to a Gertsch FM-4 multiplier, and one of the harmonics is mixed with a signal from the internal oscillator of the FM-4 multiplier to give a 10-Mc i. f. signal,

whose phase is compared with the 10-Mc signal from the AM-1 interpolator. A phase difference impresses a dc voltage across a crystal diode in the plate cavity of the 500-to 1000-Mc oscillator, thus changing the effective capacity of the oscillator tank. The 10-Mc i.f. signal is maintained exactly with respect to the AM-1 harmonic by a closed-loop adjustment of the oscillator frequency. Frequencies from 500 to 1000 Mc are generated this way.

The very accurate 100-kc signal is obtained from a JKFS-1100 1-Mc quartz-crystal oscillator (James Knight Co., Sandwick, Illinois) with a frequency divider circuit. The crystal is contained in a temperature-regulated double oven and has a stability of five parts in 10^{10} per day. This crystal is checked regularly against a standard frequency signal from National Bureau of Standards Station WWV and weekly against an "Atomicron" which is stable to one part in 10^{10} with an accuracy of one part in 10^{9}. The extreme accuracy available was not utilized in this experiment, but in the next stage of data gathering, when lines of a few kilocycles in width are encountered, the accuracy will become mandatory.

To produce the signals in the 3- to 5-k Mc range needed for the $\Delta\nu$ search, coaxially mounted crystal-diode harmonic generators are used followed by stub tuners and traveling-wave-tube amplifiers. Since the power output of the amplifiers is proportional to the input signal strength, and since the signal strength of crystal diodes falls off with higher harmonics, it is sometimes necessary to use two or more stages of frequency multiplication. One of these traveling wave tubes is shown with its power supply in Fig. 10. At times, sixteen individual pieces of equipment are in use simultaneously in generating and monitoring frequencies. In addition, there are four chassis devoted to the C-magnet stabilization system. Most of the electronic equipment as well as the magnet-regulating and beam-regulating equipment can be seen in Figs. 11 and 12.

The traveling-wave tubes seemed to generate harmonics, and it became necessary to use tunable coaxial cavities with pass bands of a few Mc as band-pass filters. Power is measured by a Wheatstone-bridge system which has a thermistor as one of its arms. Frequency is measured directly on a HP 524 frequency counter up to about 100 Mc, and indirectly above this by beating a part of the signal with a harmonic of a HP 540-B transfer oscillator. The oscillator runs from 100 to 200 Mc, and its frequency can be measured directly.

As an example, in one of the earlier runs a frequency of 5113.6 Mc was required. In order to achieve this frequency, it was necessary to multiply the fundamental frequency, 638.625 Mc, from the FM-4 interpolator eight times through two stages, with amplification after each stage. The signal from the FM-4 was obtained from a 25.9450-Mc signal from the AM-1 in the following way:

Let f_0 = 5113.6000 Mc, f_1 = 638.62500 Mc,

f_2 = 25.945.000 Mc, and f_3 = 1.945.000 Mc.

Then $f_0 = 8 \times f_1$ Mc (with crystal diode multipliers and traveling-wave-tube amplifiers)

$f_1 = 25 \times f_2$ - 10 Mc (with the FM-4)

$f_2 = 24 \times 1$ Mc + f_3 (with the AM-1)

f_3 = 1.945 Mc (taken directly from the free-running oscillator).

The accurate value of f_0 was calculated from the frequency f_3, which was counted directly.

The signal passes from the FM-4 interpolator through the entire system to the hairpin in the vacuum by means of RG-8/U coaxial cable, with a special design of vacuum feedthrough invented by N. Braslau and described in his thesis (BRA 60). The feedthrough has an insertion loss less than 3db for frequencies under 8 k Mc (Fig. 13).

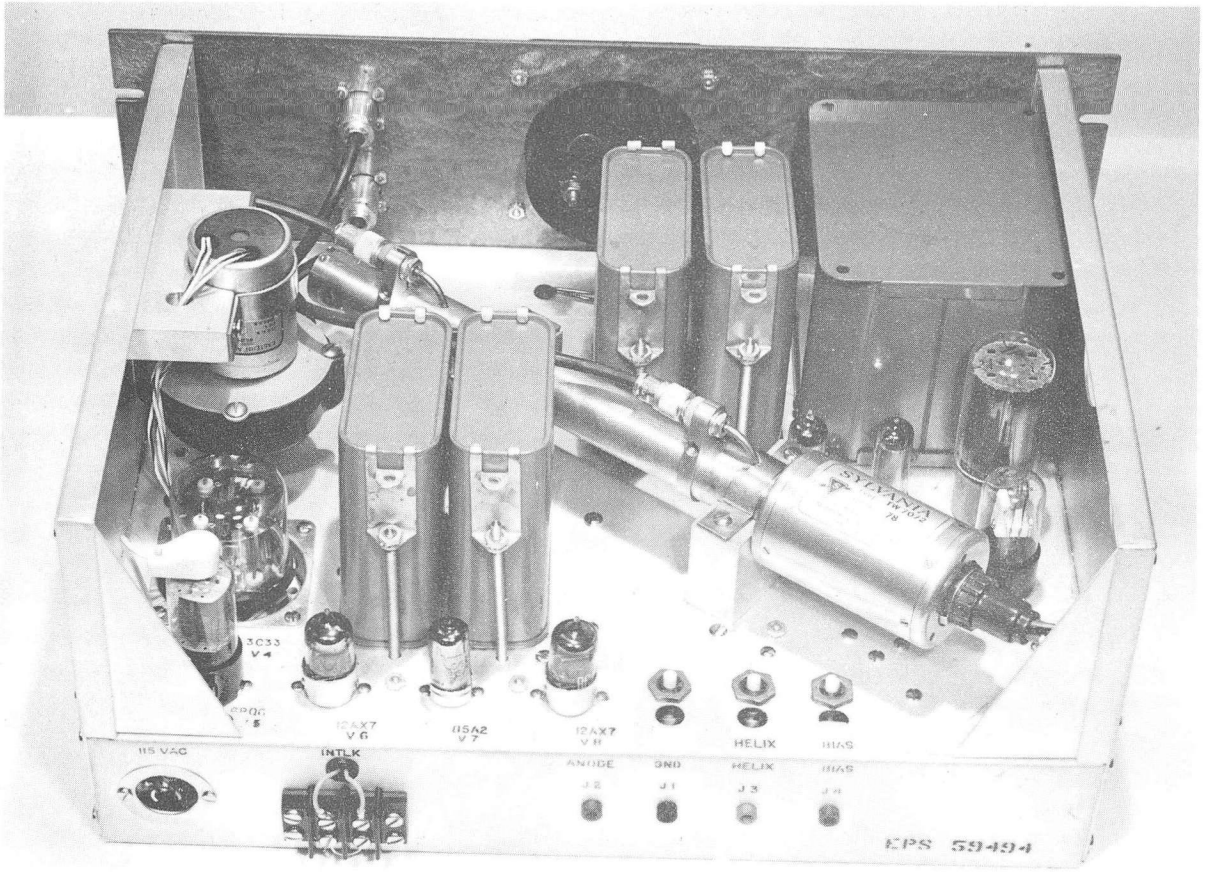

ZN-2378

Fig. 10. A traveling-wave tube.

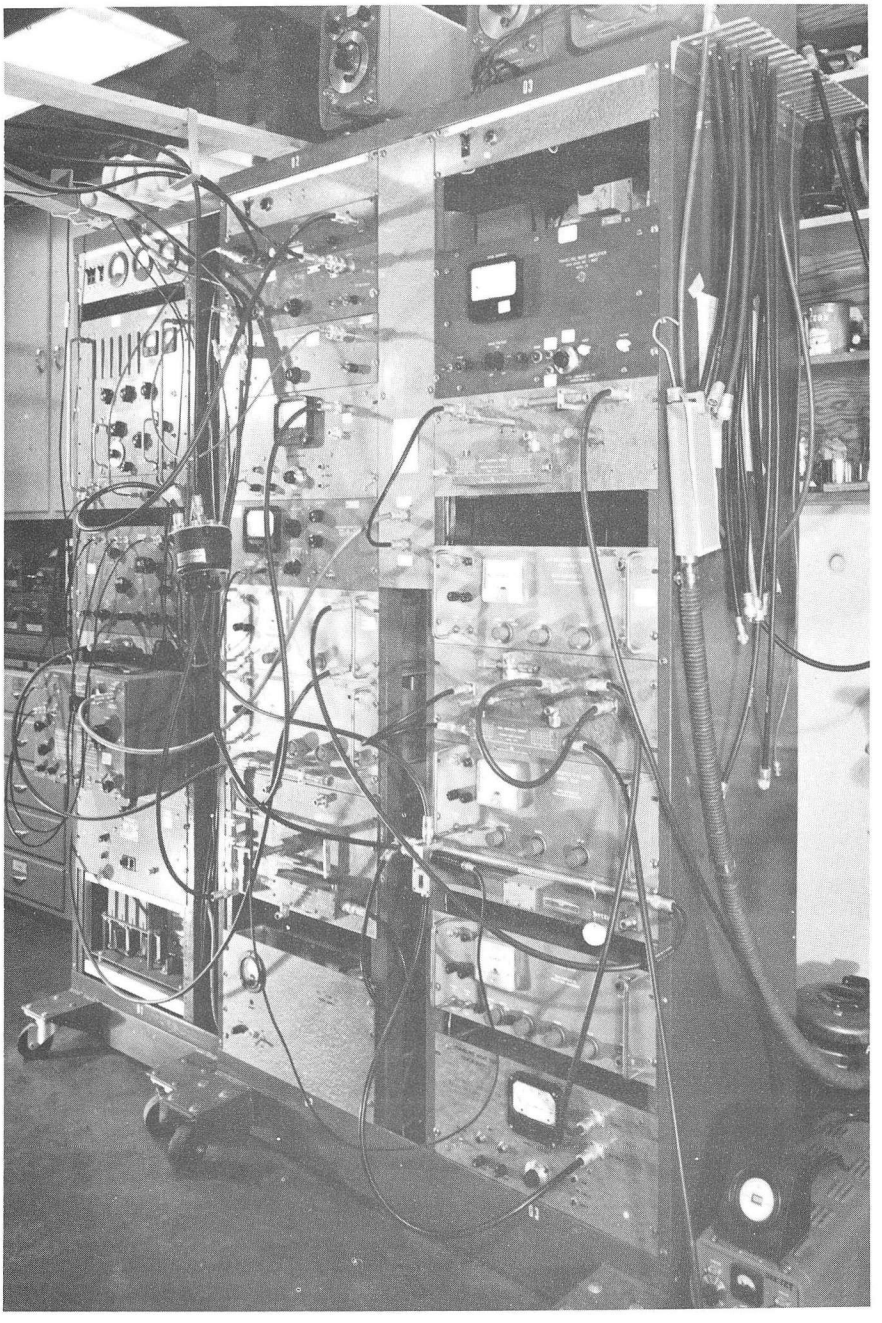

ZN-2382

Fig. 11. Frequency generating and measuring equipment.

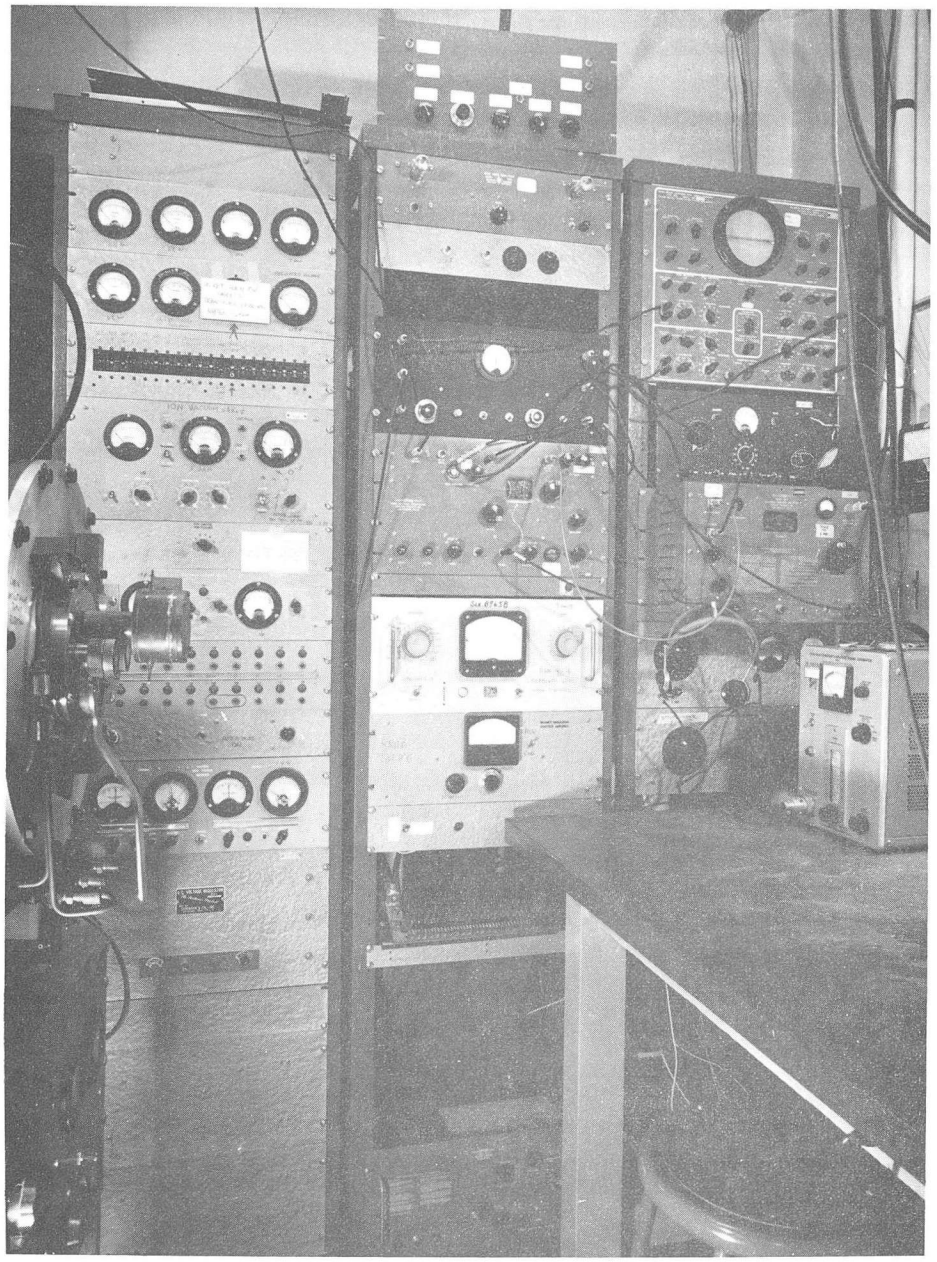

ZN-2383

Fig. 12. Magnet regulating, beam regulating, and measuring equipment.

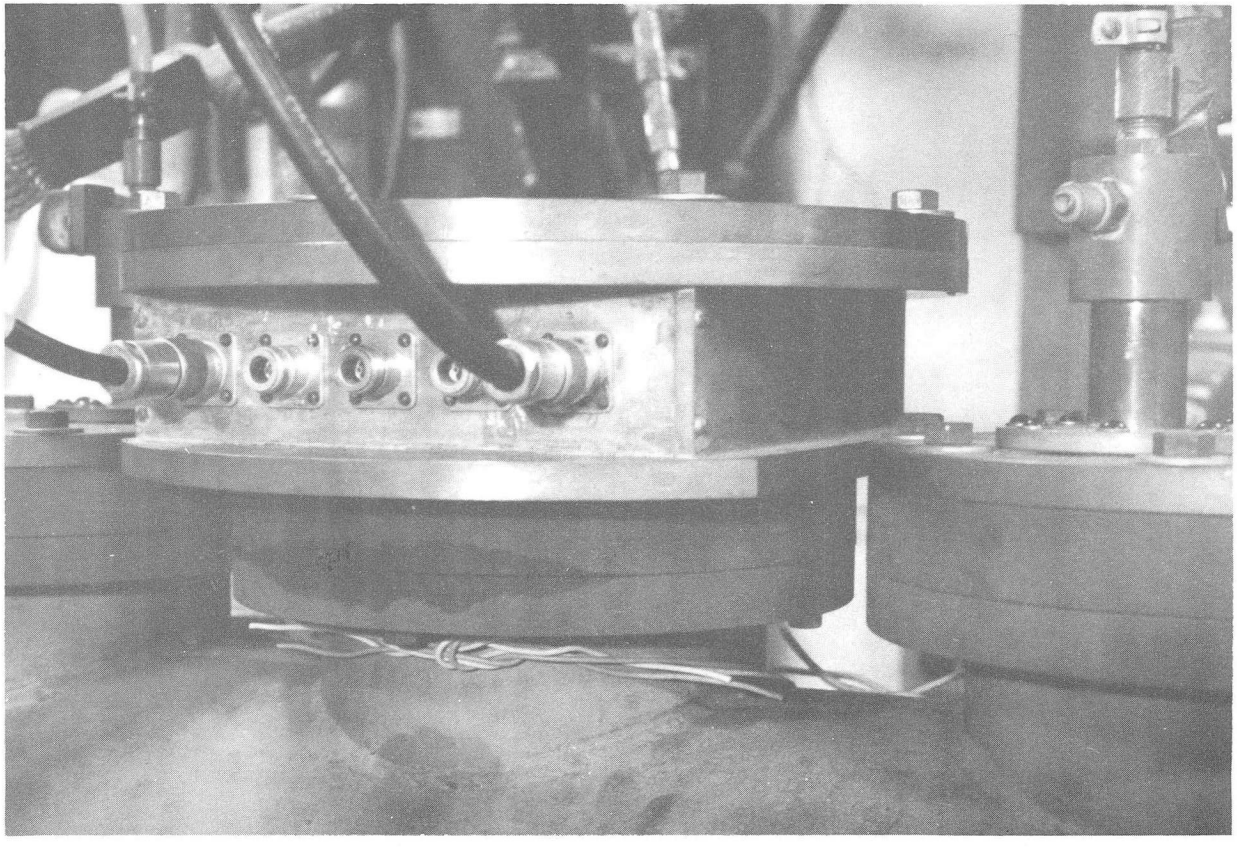

ZN-2390

Fig. 13. Radiofrequency vacuum feedthrough for coaxial cable.

Descriptions and theory of the hairpins can be found in the literature (RAM 50, RAM, 56, KUS 59, TOR 41); pictures of some of those used in this and other experiments are shown in Fig. 14. Because of their simple unshielded design, it is difficult to estimate the configuration or extent of the oscillating field which gives rise to transitions, making application of theory difficult.

Theoretically the same hairpin could be used simultaneously for both frequencies, but because of mutual-interaction problems this is impractical, making two hairpins necessary. This means that the magnetic fields are slightly different at the locking hairpin and at the search hairpin; it is necessary to use a calibrating frequency to determine exactly the field at the search region. Experience has shown that even though the fields do differ slightly in the two areas, both fields are still highly proportional to the same current producing them, and small changes in the frequency of the locking frequency are sufficient to bring the calibration frequency (and consequently the magnetic field at the search hairpin) to the required value.

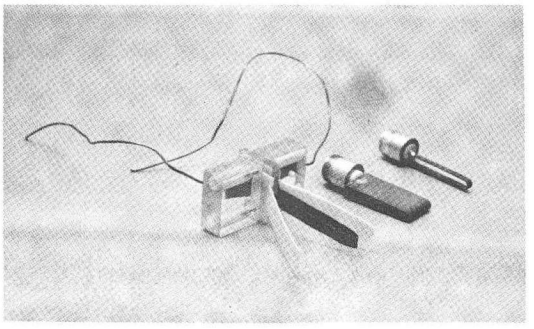

(a)

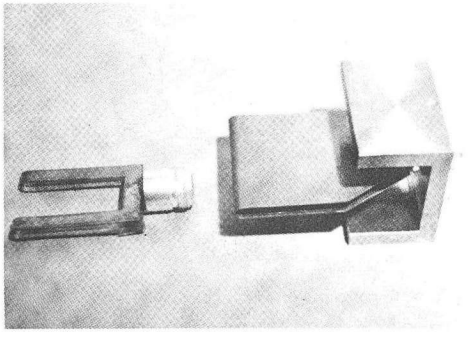

(b)

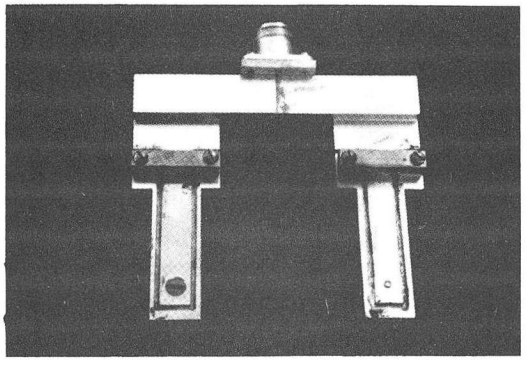

(c)

ZN-2960

Fig. 14. (a) Some simple strap hairpins.
(b) Early Ramsey hairpin designs.
(c) A later design of a Ramsey hairpin.

III. THEORY

A general description of the interaction of a nucleus with external electric or magnetic fields must have as its basis a description of its interaction with atomic and molecular fields. All measurements by various methods of nuclear resonance fit the following basic assumptions:

a. The nucleus contains a charge, +Ze, confined to a small region at the center of the atom.

b. A nucleus whose mass number A is:

1. odd obeys Fermi-Dirac statistics
2. even obeys Bose-Einstein statistics.

c. A nucleus has a spin angular momentum $\underset{\sim}{a}$ related to the spin $\underset{\sim}{I}$ by

$$\underset{\sim}{a} = \hbar \underset{\sim}{I} \qquad \text{(III.1)}$$

where $\underset{\sim}{a}$ is also called the dipole coupling constant.

d. The spin I is integral if A is even, and odd-half-integral if A is odd.

e. The nucleus has a magnetic moment, $\underset{\sim}{\mu}_I$, related to the spin by the definition;

$$\underset{\sim}{\mu}_I = \gamma_I \hbar \underset{\sim}{I} = g_I \mu_0 \underset{\sim}{I} , \qquad \text{(III.2)}$$

where μ_0 is the Bohr magneton, and γ_I and g_I are called the nuclear gyromagnetic ratio and the nuclear g factor respectively, and are defined by the above equations.

f. The atomic electrons have a magnetic moment $\underset{\sim}{\mu}_J$ related to the electronic angular momentum vector $\underset{\sim}{J}$ by

$$\underset{\sim}{\mu}_J = \gamma_J \hbar \underset{\sim}{J} = g_J \mu_0 \underset{\sim}{J} , \qquad \text{(III.3)}$$

where γ_J and g_J are obviously defined.

The magnetic interaction of the nucleus with its surrounding electrons can be described by considering the way the magnetic field at the center of the atom (that due to the electrons) affects the nuclear magnet. The nucleus is allowed certain discrete orientations in this field, each orientation having an energy level associated with it, and the transitions between these levels determine the hyperfine structure of the atom. The energy of the dipole interaction of the nucleus with its own and with external fields is

$$\mathcal{H}_m = - \underset{\sim}{\mu}_I \cdot (\underset{\sim}{H}_J + \underset{\sim}{H}_0) , \qquad \text{(III.4)}$$

where $\underset{\sim}{H}_J$ is the magnetic field due to the electrons, and $\underset{\sim}{H}_0$ is the external field either applied or due to other atoms or molecules.

A. Atomic Fields

Some information can be gained from a simpler case, e.g. when the applied field is zero. In this case Eq.(III.4) reduces to

$$\mathcal{H}_m = ha \, \underset{\sim}{I} \cdot \underset{\sim}{J} , \qquad \text{(III.5)}$$

because the field $\underset{\sim}{H}_J$ is proportional to $\underset{\sim}{J}$ and $\underset{\sim}{\mu}_I$ is proportional to $\underset{\sim}{I}$. The hfs splitting factor a, is defined by

$$ha = \frac{\mu_I}{I} \frac{\underset{\sim}{H}_J \cdot \underset{\sim}{I}}{\underset{\sim}{J} \cdot \underset{\sim}{J}} . \qquad \text{(III.6)}$$

Fermi (FER 30) calculated the field due to the electrons at a point nucleus to be

$$\underset{\sim}{H}_J = \frac{8\pi}{3} \, g_J \mu_0 \left| \psi(0) \right|^2 \underset{\sim}{J} , \qquad \text{(III.7)}$$

where $\left|\psi(0)\right|$ is the electronic wave function at the point nucleus. This is really only an approximate relationship. Then it follows that

$$ha = - \frac{8\pi}{3} \, g_J g_I \mu_0^2 \left| \psi(0) \right|^2 . \qquad \text{(III.8)}$$

Since the wave functions of electrons bound to a point nuclei are the same for two isotopes of the same element, the ratio of their hfs constants is

$$\frac{a_1}{a_2} = \frac{g_{I_1}}{g_{I_2}} , \qquad \text{(III.9)}$$

which is called the Fermi-Segrè equation.

The total angular momentum is the vector sum of the electronic and nuclear momenta,

$$\underset{\sim}{F} = \underset{\sim}{I} + \underset{\sim}{J} . \qquad \text{(III.10)}$$

This total vector $\underset{\sim}{F}$ has a magnitude F and can have components m_F along the magnetic-field direction. Here F can take on values of $I + J,\ I + J - 1,\ \cdots,\ |I - J|$; m_F can have values of $\pm F,\ \pm F - 1,\ \pm F - 2,\ \cdots$. For this set of quantum numbers, F and m_F, only the diagonal matrix elements of the energy Hamiltonian are needed, and the interaction energy becomes

$$W(F,m) = (F,m \left| H_m \right| F,m) = ha\ (F,m \left| \underset{\sim}{I} \cdot \underset{\sim}{J} \right| F,m) =$$

$$= ha\ [F(F+1) - I(I+1) - J(J+1)\ ] . \qquad \text{(III.11)}$$

The energy difference between the two adjacent states F and $F + 1$ is

$$\Delta W = W(F,m) - W(F-1,m) = \frac{ha}{2}\ [F(F+1) - (F-1)F\ ] = haF, \qquad \text{(III.12)}$$

the interval rule of hyperfine structure (RAM 53). For the alkali atoms $J = 1/2$, and F can be either $I + 1/2$ or $I - 1/2$. In this case the separation is

$$W = ha\ (I + 1/2) \equiv h\Delta\nu , \qquad \text{(III.13)}$$

where $\Delta\nu$ defined this way is called the hyperfine-structure separation.

B. External Fields

An external magnetic field causes the nuclear and electronic moments to be coupled to it. We obtain for the energy

$$\mathcal{H} = a\underset{\sim}{I} \cdot \underset{\sim}{J} - \underset{\sim}{\mu}_I \cdot \underset{\sim}{H}_0 - \underset{\sim}{\mu}_J \cdot \underset{\sim}{H}_0 \qquad \text{(III.14)}$$

$$= a\underset{\sim}{I} \cdot \underset{\sim}{J} - g_I \mu_0 \underset{\sim}{I} \cdot \underset{\sim}{H}_0 - g_J \mu_0 \underset{\sim}{J} \cdot \underset{\sim}{H}_0 .$$

There are two approximate solutions to the above equation--one for very low fields and one for very high fields. At low fields, the nuclear and electronic moments combine to give the appearance of a magnetic moment, μ_F, and off-diagonal matrix elements can be neglected, giving $2F+1$ energy levels separated by approximately $(2.8/2I+1)H$ Mc. At very high fields (the Paschen-Back region) $\underset{\sim}{I}$ and $\underset{\sim}{J}$ are completely decoupled and precess individually about the magnetic field ($\underset{\sim}{F}$ is no longer a good quantum number). In high fields solution of Eq. (III.14) then gives rise to two sets of $(2I+1)$ lines of equal separation.

The most interesting case, and the one most applicable to this experiment, is the one for intermediate fields. It is also the most difficult to analyze, since the secular equation must be solved. Because of commutation relations, all of the matrix elements of the Hamiltonian except those diagonal in $m=m_I+m_J$ will vanish, so the resulting matrix is composed of 2×2 submatrices. A straightforward solution gives the Breit-Rabi formula for the special case of $J = 1/2$

$$W(F, m_F) = (h\,\Delta\,\nu/2(2I+1)) - g_I \mu_0 H_0 m_F \pm \frac{h\Delta\nu}{2}\left[1+x^2+\frac{4m_F}{2I+1}x\right]^{1/2} \qquad \text{(III.15)}$$

where x has been substituted for $(g_I-g_J)(\mu_0 H_0/h\Delta\nu)$. (III.16)

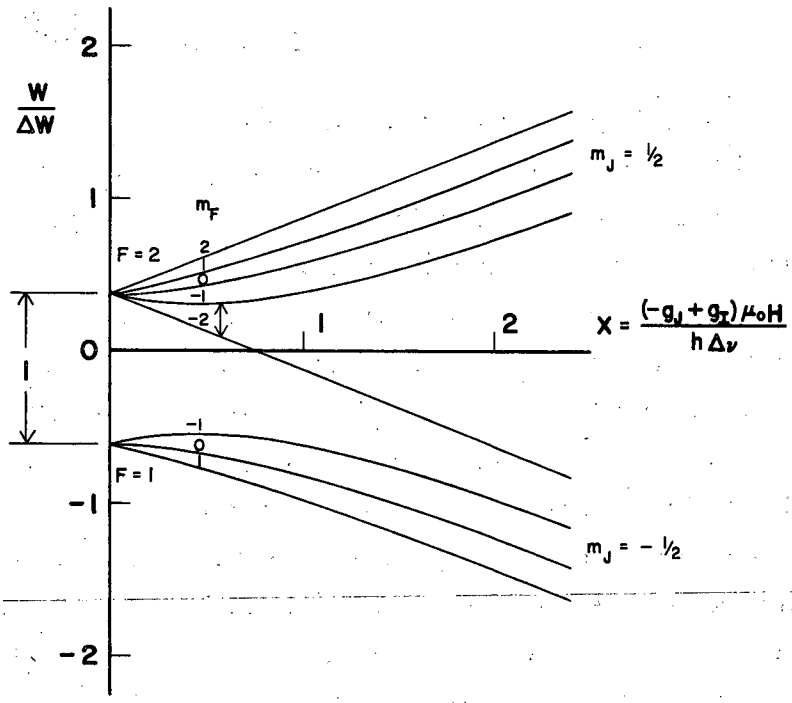

Fig. 15. Energy-level diagram for I = 3/2.

The plus sign is to be used when the atom is in the state $F = I+1/2$, the minus sign for $F=I-1/2$. Figure 15 is a Breit-Rabi energy-level diagram, for the case $I = 3/2$ (Rb^{81} and Rb^{87}). Since the quantities observed are transition frequencies proportional to the energy differences between the levels, the formula for the frequency between two levels 1 and 2 is

$$\nu_{1-2} = -\frac{g_I \mu_0 H_0}{h}(m_1 - m_2) + \frac{\Delta\nu}{2}\left\{(\pm)_1\left[1 + x^2 + \frac{4m_1}{2I+1}x\right]^{1/2} - (\pm)_2\left[1 + x^2 + \frac{4m_2}{2I+1}x\right]^{1/2}\right\}. \qquad \text{(III.17)}$$

Note that $(\pm)_1$ equals $-(\pm)_2$ when m_1 and m_2 belong to different F (the usual case), and $(\pm)_1$ equals $(\pm)_2$ when they belong to the same F.

C. The Force on the Atom

The force on an atom in an inhomogeneous magnetic field is proportional to the inhomogeneity of the field and to the strength of the magnetic moment along the field:

$$\underset{\sim}{F} = -\nabla W = -(\partial W/\partial H)\nabla H = \mu_{eff}\nabla H, \qquad \text{(III.18)}$$

where μ_{eff} is the component of $\underset{\sim}{\mu}$ along H. For very large fields, when m_I and m_J are good quantum numbers, we have

$$\mu_{eff} \cong g_J \mu_0 m_J + g_I \mu_0 m_I . \qquad \text{(III.19)}$$

Since g_I is much smaller than g_J, for $J = 1/2$ the effective moment is essentially either μ_0 or $-\mu_0$, regardless of the nuclear substate. The fields in the A and B focusing magnets are high enough for this to be true. Thus an atom in the inhomogeneous field of the A-magnet finds itself in a state aligned either with or against the magnetic field. In

this orientation it experiences a force either along the direction or against the direction of the field. The atom tends to follow an arc of a parabola. The atoms emerging from the oven in certain directions are permitted to pass through the apparatus. The field in the C-magnet is usually considerably smaller than that in the A- and B-magnets, and it is quite homogeneous. The fringe fields from the A- and B-magnets somewhat extend in space toward the field of the C-magnet so that the atoms never leave a magnetic field and therefore never have a chance to lose their initial orientation. The three fields are arranged so that their polarities are the same, otherwise there could be a small fieldless region on each side of the C-field. In this region some of the atoms would lose their orientation and would likely end up in a different substate (MAJ 32).

There are two directions for the B field inhomogeneity, and both of them have been used. Historically, the first direction was opposite to that in the A-magnet field. This puts the force on a particular atom in the opposite direction from that experienced in the A-magnet field. Thus if nothing happened to the atom in the C-magnet field, it would be forced back to the center line of the machine (i.e., would be refocused) and would strike the detector. If the atom could be induced to change its electronic substate so that its effective moment would then be in the opposite direction, the force in the oppositely directed gradient of the B-magnet field would be the same as in the A-magnet, and the atom would be deflected out of the main beam path. A resonance thus appears as a decrease in beam intensity. For work on radioactive atoms this is an unsatisfactory method because of the statistics involved in radioactive counting. The second method overcomes this difficulty because the gradient is in the same direction as that of the A-magnet. In this case, if nothing happens to an atom as it travels between the A-magnet and the B-magnet, it will continue to the deflected in the same direction and will be pushed away from the center line just as the "flopped" atoms in the first method were. If the effective moment of the atom is

changed, however, it will then be refocused. Thus no signal is seen at the detector unless a change in effective moment occurs. Therefore the small radioactive signal can now be seen above a relatively small background. This latter method, called the "flop-in" method, is used in this and all modern experiments on radioatoms.

D. Induced Transitions

The transitions between the different substates can be considered as being induced by the oscillating magnetic part of the electromagnetic field. The field, $\underset{\sim}{H}_1 \cos 2\pi\nu t$, is superimposed upon the static C-magnet field, $\underset{\sim}{H}_0$, where H_1 is the magnitude of the oscillating field, and $h\nu$ is the energy of the quantum. This adds to the energy Hamiltonian, Eq. (III.14) a time-dependent term

$$V = \mu_0 g_J \underset{\sim}{J} \cdot \underset{\sim}{H}_1 \cos 2\pi\nu t + \mu_0 g_I I \cdot H \cos 2\pi\nu t. \qquad \text{(III.20)}$$

Rabi in 1937 showed that the following selection rules result from the above perturbation at low field (RAB 37, KUS 59):
for the component of H_1 parallel to H_0,

$$\Delta F = 0, \pm 1; \quad \Delta m_F = 0 \qquad \text{(III.21B)}$$

for the perpendicular component,

$$\Delta F = 0, \pm 1; \quad \Delta m_F = \pm 1 \qquad \text{(III.21B)}$$

In high fields, where F is not a good quantum number, the rules are

$$\Delta m_J = 0; \quad \Delta m_I = 0 \qquad \text{(III.22A)}$$

for the parallel component, and

$$\Delta m_J = 0, \pm 1; \quad \Delta m_I = 0, \pm 1 \qquad \text{(III.22B)}$$

for the parallel component. To be refocused, the atom must undergo a $\Delta m_J = \pm 1$ transition, since this causes a change in effective moment in the deflective fields. A look at the Breit-Rabi diagram (Fig. 15)

shows that there is only one transition at frequencies much less than $\Delta\nu$ which satisfies the refocusing condition ($F = +I + 1/2$, $m_F = -I + 1/2 \longleftrightarrow F = I + 1/2$, $m_F = -I - 1/2$). Equation (III.17) shows the frequency of this transition to be

$$\nu \cong 2.8 H_0/(2I+1) . \tag{III.23}$$

If two isotopes are together in the beam and the spin of one is known, Eq. (III.23) can be used to find the other at very small fields:

$$\nu_1 = \nu_2(2I_2 + 1) / (2I_1 + 1) . \tag{III.24}$$

When the spin is known, the H_0 field can be increased and the transition followed so that the quadratic field dependence of the transition frequency can be observed. Denoting the frequency in Eq. (III.23) as ν_z, the Zeeman frequency, and expanding Eq. (III.17) to include quadratic terms in H_0, we get for the frequency in megacycles per second

$$\nu = \nu_z + (\nu_z)^2 \frac{2I}{\Delta\nu} , \tag{III.25}$$

which confirms the spin and places a lower limit on $\Delta\nu$.

As $\Delta\nu$ becomes known more accurately, higher values of H_0 must be used, and it becomes necessary to employ the exact solution of Eq. (III.17):

$$\Delta\nu = \frac{\left(\nu + \frac{g_I\mu_0 H_0}{h}\right)\left(-\nu - \frac{g_J\mu_0 H_0}{h}\right)}{\nu + \left(\frac{2I}{2I+1} \cdot \frac{g_I\mu_0 H_0}{h}\right) + \left(\frac{1}{2I+1} \cdot \frac{g_J\mu_0 H_0}{h}\right)} \tag{III.26}$$

where ν is the observed frequency, and g_I is the only quantity that is not either known or observable. It can be found within a few percent by using the Fermi-Segrè formula, Eq. (III.9). However, without prior knowledge, we have no way of knowing whether g_I is positive or negative, and we must assume each in turn. Thus, as the field increases, the uncertainty in

$\Delta\nu$ becomes less and less, and the value of $\Delta\nu$ will be consistent for only one choice of sign.

When $\Delta\nu$ is known to within a few megacycles, the field is reduced to a very low value, and a search begins for the $\Delta F = \pm 1$ transitions that have frequencies approximately equal to $\Delta\nu$. Since the hairpins used are capable of producing a strong H_1 field only in the direction perpendicular to H_0, only transitions satisfying $\Delta m_f = \pm 1$ are observed. There are $2I-1$ of these lines separated by twice the Zeeman frequency, ν_z. All but the highest line are unresolved doublets; the highest is a singlet. When I is integral, as in Rb^{82}, the central doublet is very close to $\Delta\nu$, there being only a few kc correction due to second-order field terms in Eq. (III.17). Observation of this field-independent line will give $\Delta\nu$ to an accuracy limited only by the resonance half-width and the shape of the line. If I is odd-half-integral, as in Rb^{81}, this field-independent line can be excited only by an H_1 parallel to H_0, and we are forced to observe field-dependent lines which have a linear dependence on the field. If it is possible to observe both transitions, one Zeeman frequency above and below $\Delta\nu$, the average of these frequencies will differ from $\Delta\nu$ by only a few kilocycles. In this case the accuracy of the line will be determined by the half-widths of the resonances.

Any of the lines that lie below $\Delta\nu$ must go through a minimum frequency at a higher field where the line spread due to field broadening will be small. If the width of the lines becomes small enough, it may be possible to resolve the doublet lines. Designating the higher line as ν^+, and the lower as ν^-, we find that their separation,

$$\nu^+ - \nu^- = \left| g_I \right| (2\mu_0 H_0/h) \qquad \text{(III.27)}$$

is proportional to g_I and H_0. We can then determine g_I as accurately as resolution of the apparatus permits. Accuracies as great as one part in 10,000 are possible and one in 1000 has been achieved in this laboratory (BRA 60).

IV. EXPERIMENTAL TECHNIQUES

The neutron-deficient isotopes of rubidium are readily obtainable at this laboratory. The half-lives of the two lightest, Rb^{81} and Rb^{82}, are about 5 hr. This is not so short as to preclude reasonable chemistry and machine warm-up periods but short enough so that reasonable numbers of atoms will be counted. In conjunction with other work done here, these isotopes will help to complete information on the chain of adjacent rubidium isotopes from Rb^{81} to Rb^{88}.

A. Chemistry

The isotopes are produced by bombarding $BaBr_2$ with 48-Mev alpha particles for about 4 hr in the 60-in. cyclotron on the University of California campus at Berkeley. Since the cyclotron is about 100 yd from the caves where the chemistry was performed, the targets are brought from the cyclotron to the caves in mobile lead target carriers.

The chemistry was performed in a standard lead-shielded cave box. The target was disassembled and the $BaBr_2$ powder washed from its holder into a test tube in which about 75 mg of RbBr was placed to act as a carrier during the chemistry as well as provide stable rubidium in the beam for calibration and locking. Ammonium carbonate was added to precipitate the barium until, after centrifuging, no more barium came out. The clear solution containing stable and radioactive rubidium ions, as well as bromide, ammonium, and carbonate ions was then heated gently to remove the excess carbonate ions in the form of CO_2. Upon heating, the water evaporated, leaving ammonium bromide and rubidium bromide crystals. Further heating in an electric furnace sublimed the ammonium bromide. The anhydrous crystals of rubidium bromide were then scraped from the walls of the test tube and placed in the steel oven along with fresh calcium filings. The oven cap was pressed into place, and the oven removed from the cave and placed in the oven loader of the beam machine.

B. BEAM PRODUCTION

One to 1-1/2 hr was required to obtain a satisfactory beam of atoms. About half the time was spent in evacuating and loading the oven into the oven-chamber, and the rest of the time in heating the oven to allow the chemical reaction to proceed. After the oven filament reached operating temperature, the electron power was increased to a few watts, then slowly increased to about 10 or 15 w and held at this level for some time. During this time, the pressure was observed to rise gradually, level off, and then drop rather quickly to about the region that existed during the previous run (usually about 5 to 8×10^{-6} mm Hg). Shortly after the pressure dropped, a beam was observed on the hot-wire detector. The rate at which it developed indicated whether it would equilibrate at a high or low level, and the power was adjusted accordingly to achieve the level desired for the particular run. When the beam had reached a fairly stable level, a sulfur-coated button was introduced for five minutes into the beam path. The counting rate of the "full-beam" button then gave an estimate of the expected counting rate of the resonance buttons. The beam could be controlled by increasing or decreasing the electron bombardment power. The full-beam button was exposed with all magnets off and the stop wire removed.

C. BEAM DETECTION

The atoms that passed through the apparatus were collected on sulfur buttons, were then sent up three floors through a pneumatic tube to a counting room at the opposite corner of the building. The buttons were placed in crystal counters which detected their K-x-rays as described in Section II. Full-beam counting rates of 200 to 300 counts per minute (cpm) were not uncommon, with the resonance buttons running from 3 to 5 cpm. The backgrounds of the counters are about 1 to 2 cpm; therefore the results were generally satisfactory for 10-min exposures. Since Rb^{81} and Rb^{82} were the only isotopes produced in sufficient numbers to register above the counter background, and since

their $\Delta \nu$ values were so different, there was no identification problem, although pulse-height analyses of chemistry samples and full-beam buttons were run in the later stages of the experiment for completeness.

D. EXPERIMENTAL PROCEDURE

After the beam intensity had reached a stable level the oven was aligned. The exit-slit detector was placed on the center line of the machine and the oven rotated and moved laterally until the beam showed a maximum, usually about 2×10^{-10} amp. The stopwire was then inserted into the beam and the detector moved to each side in succession to determine the intensity of the part of the beam that was not shadowed by the stopwire. Figure 16 is the profile of the beam with the stopwire in and out. If there were any deviations from this profile, the oven was moved slightly until the beam shape became symmetric. The oven was then considered aligned with the oven slit on the center line of the apparatus and with the direction of the beam down the center line. The full beam could be measured (with stopwire out of the beam path) at the botton loader by moving the exit detector laterally.

When the beam was properly aligned and the intensity of the beam was stable, the full-beam sample was taken, as previously mentioned, and the power was adjusted further as necessary. The full beam was then measured at the exit slit and monitor detectors, the A- and B-magnet current turned on, the stopwire put back in the beam, the monitor detector moved to the side until it was at the position of the maximum number of flopped-out atoms, and the reading of the monitor detector recorded along with the full-beam readings. Figure 17 shows the profile of the monitor detector with the magnets off, and with them on with the stopwire in and out. The relative intensity of the stable beam (and therefore of the radioactive beam except for half-life decay) could be determined merely by noting the monitor reading.

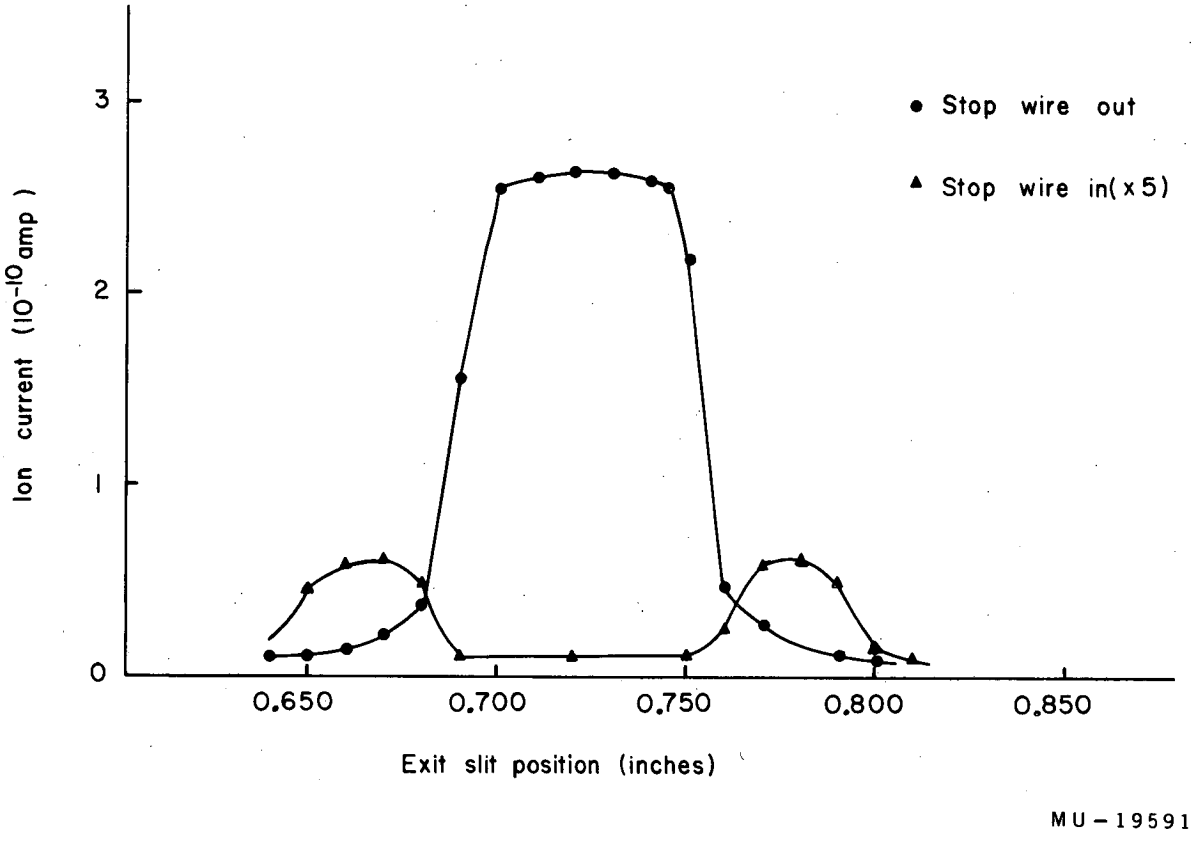

Fig. 16. Beam profile with stopwire in and out.

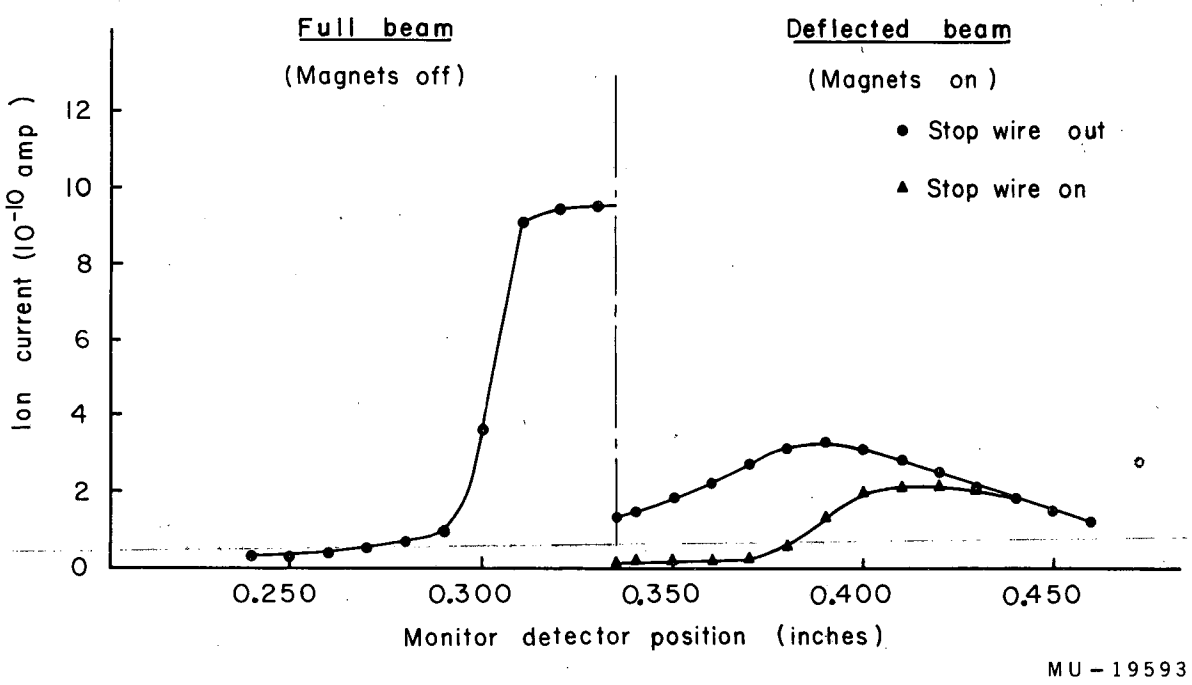

Fig. 17. Beam profile with magnets off, and with magnets on and the stopwire in and out.

The C magnet was degaussed by alternately reversing the full current through the magnet, gradually reducing the current until the approximate desired field and proper orientation of field were obtained. The locking rf signal was then sent into the hairpin, and the field adjusted manually until the resonance was seen. The locking device was placed in operation to maintain the required field. Occasionally the field changes were too great for the locking device to handle, and some manual control was necessary. The rf power was adjusted for optimum operation of the locking system. The calibrating frequency was then sent into the search hairpin and varied slightly until the calibrating resonance was seen on top of the locking flop. The calibration frequency was then measured, and the field at the site of the search hairpin calculated. Small changes were made in the locking frequency to bring the field at the search hairpin to the proper value, and we were ready to being the run.

To provide some idea of the sort of background from stray atoms at the detector, an "apparatus background" (zero rf) button was used as a reference. Next, a search signal of a particular frequency was introduced into the search hairpin, and a button placed in line with the beam at the detector end. The time of exposure was varied to suit the counting rate of the full-beam button, usually about 10 min. At the end of the exposure, the button loader was rotated a quarter turn to take the button out of the beam, and the frequency was changed. The exposed button was then rotated to the rough pump-out region, while a new button was introduced into the beam. The rough pump-out region was raised to atmospheric pressure and the exposed button was removed and sent to the counting room.

Periodically during the run the button loader hot-wire detector was rotated into position and the field recalibrated. At the end of a run, if the beam had not dropped too low, the monitor reading was compared again with the full beam with magnets off and stopwire out. The readings over a period indicated good consistency, even though one or the other filaments were changed from time to time. The reading of the monitor

detector was observed several times during each exposure and recorded in the run book to be used in normalizing the counting rates. The buttons were counted immediately after exposure, and their counting rates (with machine and counter background subtracted off) plotted against their frequencies. The resonances were then fitted by eye, and by an IBM 650 routine OMNIBUS (SHU 57), to obtain the central frequency and the estimated uncertainty.

V. EXPERIMENTAL RESULTS

A. Measurement of $\Delta\nu$

The spin and rough value of $\Delta\nu$ and the sign of the moment for both Rb^{81} and Rb^{82} given by Hubbs et al. (HUB 57, SHU 57) are:

$\underline{Rb^{81}}$ $I = 3/2$

$\Delta\nu = 5097 \pm 13$ Mc

g_I positive

$\underline{Rb^{82}}$ $I = 5$

$\Delta\nu = 3094.1 \pm 2.4$ Mc

g_I positive.

The uncertainty in $\Delta\nu$ for Rb^{81} was reduced by observing the $\Delta F = 0$ transition at a field of 591.4 gauss. In this case, the uncertainty was reduced to 8 Mc, whereupon an attempt was made to see a $\Delta F = \pm 1$ transition in the Zeeman region at 4 gauss. When a line is seen, at first its identity is unknown. Some method must be used to determine which of the many possible lines has been measured. In Rb^{81} there are three observable transitions in the $\Delta\nu$ region. In Rb^{82} there are ten! There are two ways to determine which line has been observed. The first is to calculate the separation of the lines for the particular field, expose a button at the proper frequencies above and below the observed line, and see whether the counting rate is high or low. A high rate indicates that a line should be found at that frequency; a rate comparable to machine background indicates no line. A difficulty in this method is that the counting rates are already low, and it is sometimes difficult to ascertain whether the rate for a button is truly high, or perhaps just a statistical fluctuation. A wrong assignment in the early work was the result of such a statistically high counting rate. After this mistake, a better and surer method was used, namely shifting the H_0 field a small amount and observing the corresponding shift in the center frequency of the resonance. When the identification was positive in

Rb^{81}, the lines immediately above and below $\Delta\nu$ were examined at the same field. The value of $\Delta\nu$ was determined by averaging the frequencies of these lines, since their average is only 5 kc above $\Delta\nu$ at the field in which these lines were observed. Figure 18 shows these two resonances. The value of the hfs separation as determined from these two lines is

$$\Delta\nu_{81} = 5111.589 \pm .040 \text{ Mc.}$$

When the identification of the line for Rb^{82} was clear, buttons were exposed in the region where $\Delta\nu$ was expected to be. A line 40 kc wide was observed, and when the field was shifted, the line remained at the same frequency, confirming that it was indeed the field-independent $\Delta\nu$ transition. The value of the hfs separation for Rb^{82} was then determined to be

$$\Delta\nu_{82} = 3094.084 \pm .006 .$$

Figure 19 shows one of the $\Delta\nu$ transitions. Tables I and II summarize all the data for the important runs.

B. Preliminary Measurement of the Moment of Rb^{81}

In the last successful run of this experiment, the two lines of the resolved doublet, in its field-independent region of 488.5 gauss, were observed. From Eq. (III.26), we have $g_I = (\nu^+ - \nu^-)/(2\mu_0 H_0/h)$ and the expected $(\nu^+ - \nu^-)$ is within 1% of 1.0213 Mc. The observed transitions were at 4936.90±.15 Mc and 4938.10±.15 Mc, with a difference of 1.20±.22 Mc. This is somewhat higher than should be expected. Later experiments may improve this value.

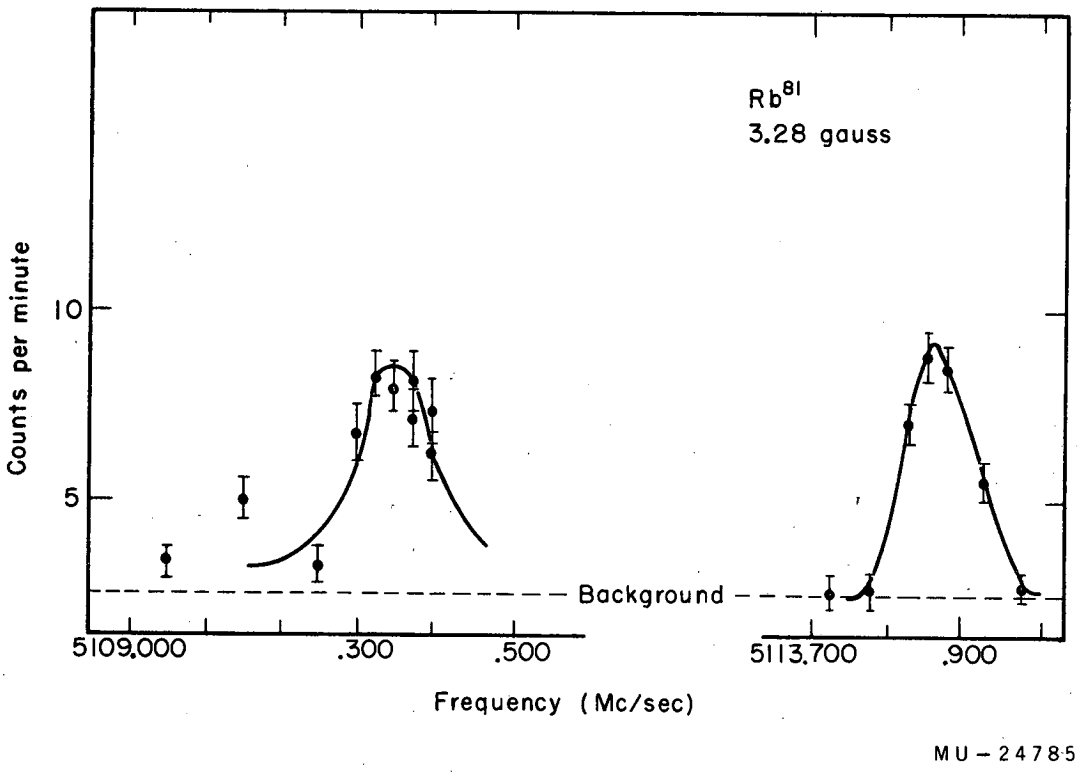

Fig. 18. The $\left\{\begin{matrix}2,0 \longleftrightarrow 1,-1 \\ 2,-1 \longleftrightarrow 1,0\end{matrix}\right\}$ and $\left\{\begin{matrix}2,0 \longleftrightarrow 1,1 \\ 2,1 \longleftrightarrow 1,0\end{matrix}\right\}$ resonances in Rb^{81}.

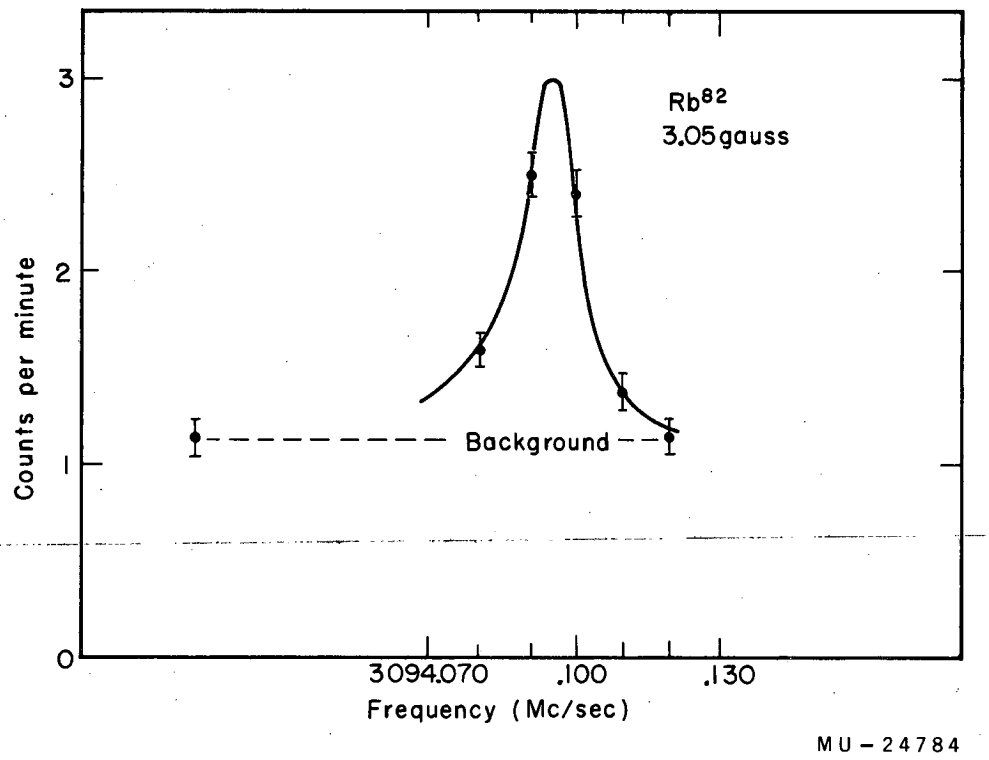

Fig. 19. The (11/2, 1/2 $\longleftrightarrow$ 9/2, -1/2) transition in Rb^{82}.

Table I. Summary of data for Rb^{81}

Run	$\nu(Rb^{81})$ (Mc/sec)	$\nu(Rb^{87})$ (Mc/sec)	Calculated $\Delta\nu$[a] (Mc/sec)	$m_1 \leftrightarrow m_2$
$F_1 = 2$ to $F_2 = 2$ transition				
55	531.1(2)	456.95(3)[b]	5112(8)	$-1 \leftrightarrow -2$
$F_1 = 2$ to $F_2 = 1$ transitions				
71	5113.6(5)	2.11(1)	5111.4(5)	$1 \leftrightarrow 0$ or $0 \leftrightarrow 1$
73	5113.7(2)	2.11(1)	5111.7(2)	$1 \leftrightarrow 0$ or $0 \leftrightarrow 1$
140[c]	5113.680(25)	2.10(1)	5111.569(42)	$1 \leftrightarrow 0$ or $0 \leftrightarrow 1$
143[c]	5113.690(25)	2.09(1)	5111.579(61)	$1 \leftrightarrow 0$ or $0 \leftrightarrow 1$
145A[c, d]	5113.870(63)	2.30(8)	5111.548(53)	$1 \leftrightarrow 0$ or $0 \leftrightarrow 1$
145B[c, d]	5109.335(24)	2.30(8)	5111.632(24)	$0 \leftrightarrow -1$ or $-1 \leftrightarrow 0$
168	4936.90(15)	3106.02(3)[e, b]		$0 \leftrightarrow -1$
173	4938.10(15)	3106.04(3)[e, b]		$-1 \leftrightarrow 0$

a. The least-squares fit of all resonances gives $\Delta\nu = 5111.589(40)$ Mc/sec.

b. The value of ν given here is for Rb^{85}.

c. The weighted average of runs 140, 143, 145A, and 145B gives $\Delta\nu = 5111.566(30)$.

d. The average of runs 145A and 145B corrected for second-order field effects is $\Delta\nu = 5111.597(40)$ Mc/sec.

e. The calibration transition in Rb^{85} is $F, m = 3, 3 \rightarrow 2, 2$.

Table II. Summary of data for Rb^{82}

Run	ν (Mc/sec)	$\nu(Rb^{87})$ (Mc/sec)	Calculated $\Delta\nu$[a] (Mc/sec)	$11/2, m_1 \leftrightarrow 9/2, m_2$	
67A	3098.6(3)	2.19(3)	3093.8(4)	7/2	5/2
67B	3100.3(3)	2.19(3)	3093.9(4)	9/2	7/2
81	3098.80(10)	2.14(2)	3094.0(1)	7/2	5/2
88A	3098.70(5)	2.10(2)	3094.10(6)	7/2	5/2
88B	3099.03(10)	2.26(2)	3094.08(10)	7/2	5/2
88C[b]	3094.098(10)	2.26(2)	3094.086(10)	1/2	-1/2
96	3094.083(15)	2.26(2)	3094.071(15)	1/2	-1/2
109A[b]	3094.094(5)	2.045(5)	3094.084(5)	1/2	-1/2
109B[b]	3094.097(10)	2.12(3)	3094.086(10)	1/2	-1/2

a. The least-squares fit of all resonances gives $\Delta\nu$ = 3094.084(6) Mc/sec.

b. Runs 88C, 109A, and 109B indicate $\Delta\nu$ = 3094.085(6) Mc/sec.

ACKNOWLEDGMENTS

I would like to thank everyone who assisted in completing this experiment. Specifically, I would like to thank:

Professor William A. Nierenberg, my research director, whose enthusiasm led me to pursue this line of research,

Professor Howard A. Shugart, whose guidance and personal touch saved many an experiment from failure,

Drs. Gilbert O. Brink and Norman Braslau who conceived the machine and did the major work in designing and constructing it,

Messrs. Jhan Khan and Richard Worley for their help in running the experiments,

Messrs. Michael Devito and Ralph Stein for counting and keeping the research room in order.

In addition I would also like to thank the rest of the Atomic Beams Group, especially Dr. W. Bruce Ewbank, for their continued support, the many people on the staff of the 60-in. cyclotron, and the Health Chemists who looked after my safety.

This work was done under the auspices of the U. S. Atomic Energy Commission and supported in part by the National Science Foundation.

APPENDIX: CONSTANTS USED IN THIS WORK

The values of the physical constants used in this work have been taken from E. R. Cohen, K. M. Crowe, and J. W. M. duMond, The Fundamental Constants of Physics (Interscience Publishers, New York, 1957):

$$h = 6.62517(23) \times 10^{-27} \text{ erg sec},$$

$$\mu_0 = 9.2731(2) \times 10^{-21} \text{ erg/gauss},$$

$$k = 1.38042(10) \times 10^{-16} \text{ erg/deg},$$

$$M_p/m_e = 1836.12(2),$$

$$\mu_N = \mu_0(m_e/M_p) = 5.05038(18) \times 10^{-24} \text{ erg/gauss}.$$

The constants for the calibration isotope, Rb^{87}, are:

$g_J = -2.00238(2)$	(KUS 49)
$\Delta\nu = 6834.7005(11)$Mc	(BED 52)
$g_I = 9.95259 \times 10^{-4}$	(YAS 51)
$I = 3/2$	(KOP 33)

REFERENCES

BED 52 B. Bederson and V. Jaccarino, Phys. Rev. 87, 228 (1952).

BEM 53 G. Bemski, The Fluorine Resonance in Molecular Beams, thesis, University of California, Sept. 1953 unpublished.

BRA 60 Norman Braslau, The Rubidium 85-Rubidium 86 Hyperfine-Structure Anomaly, thesis, UCRL-9130, June 1960.

BRI 59 G. O. Brink and N. Braslau, Rev. Sci. Instr. 30, 670 (1959).

FER 30 E. Fermi, Z. Physik 60, 320 (1930).

HUB 57 J. C. Hubbs, W. A. Nierenberg, H. A. Shugart, H. B. Silsbee, and R. J. Sunderland Phys. Rev. 107, 723 (1957).

KOP 33 H. Kopfermann, Naturwiss. 21, 24 (1933).

KUS 49 P. Kusch and H. Taub, Phys. Rev. 75, 1477 (1949).

KUS 59 P. Kusch and V. W. Hughes, Handbuch der Physik, Vol 37, No. 1 p. 1., Editor, E. Flügge, (Springer-Verlag, Berlin, 1959).

MAJ 32 E. Majorana, Nuovo cimento 9, 43 (1932).

RAB 37 I. I. Rabi, Phys. Rev. 51, 652 (1951).

RAM 50 N. F. Ramsey, Phys. Rev. 78, 695 (1950).

RAM 53 N. F. Ramsey, Nuclear Moments, (John Wiley and Sons, New York, 1953).

RAM 56 N. F. Ramsey, Molecular Beams, (Clarendon Press, Oxford, 1956).

SHU 57 Howard A. Shugart, The Nuclear Spins, Hyperfine-Structure Separations, and Magnetic Moments of Cs^{127}, Cs^{129}, Cs^{130}, and Cs^{132}, thesis, UCRL-3770, June 1957.

SMI 59 K. F. Smith, Molecular Beams (Methuen and Co., London, 1959).

SUN 56 : Robert J. Sunderland, The Nuclear Spins of Rb^{82}, Rb^{83}, and Rb^{84}, (thesis), University of California, June 1956 (unpublished).

TOR 41 H. C. Torry, Phys. Rev. 59, 293 (1941).

YAS 51 E. Yasaitis and B. Smaller, Phys. Rev. 82, 750 (1951).

ZAC 42 J. R. Zacharias, Phys. Rev. 61, 270 (1942).